MAGNETOSTATIC SURFACE WAVE

MICROWAVE OSCILLATOR

THESIS

AFIT/GE/EE/81D-35   Philip W. Linke
                          Captain   USAF

DTIC
ELECT
JUN 1 5 1982

E

AFIT/GE/EE/81D-35

MAGNETOSTATIC SURFACE WAVE
MICROWAVE OSCILLATOR

THESIS

Presented to the Faculty of the School of Engineering

of the Air Force Institute of Technology

Air University

in Partial Fulfillment of the

Requirements for the Degree of

Master of Science

by

Philip W. Linke

Captain   USAF

Graduate Electrical Engineering

18 December 1981

Preface

In November 1980, Sethares and Stiglitz, of the Air Force Cambridge Research Laboratories (AFCRL), New Bedford, Massachusetts, presented a paper at the 1980 Annual Conference on Magnetism and Magnetic Materials which dealt with using magnetostatic wave technology in the fabrication of a delay line for use in feedback loop of a 2-4 Gigahertz (GHz) amplifier (Ref. 13). Thin film yttrium-iron-garnet (YIG) was used as the propagation medium and the three principal modes of propagation, surface, forward volume, and backward volume waves, were investigated.

In January, 1981, I was introduced to the AFCRL work as a possible thesis topic by my thesis advisor, Capt Roger Colvin, professor of electrical engineering at the Air Force Institute of Technology (AFIT). It was determined that my task was to advance the AFCRL research by investigating the tuning rate of such an oscillator, its quality factor, and two phenomenona known as multimoding and mode hopping that occur as the oscillator is tuned. I was limited to working on just the surface wave propagation mode because of equipment and time limitations.

Because this was primarily an experimental effort, I am deeply indebted to those individuals who supported me throughout this effort. Specifically, I would like to thank

Contents

List of Figures

List of Tables

Notation

Symbol	Meaning
AFCRL	Air Force Cambridge Research Laboratory
AFIT	Air Force Institute of Technology
ATC	Air Training Command
B	Magnetic flux density
BW_3	3dB noise bandwidth
f_0	Frequency of oscillation
H	Magnetic field intensity
H_a	Anisotrophy field intensity
H_d	Demagnetizing field intensity
H_{DC}	DC bias field intensity
H_{RF}	RF input field intensity
IL	Delay line insertion loss
k	Magnetostatic wave vector number
MSSW	Magnetostatic surface wave
MSW	Magnetostatic wave
N	Number of turns in coils one and two
N_d	Demagnetization factor
Q	Quality factor
s_k	Sign of magnetostatic wave vector number
T	Period of coils one and two current
t_0	Delay associated with electrical components in feedback loop
YIG	Yttrium-iron-garnet

γ	Gyromagnetic ratio
Δf_{BP}	Shift in delay line bandpass
Δf_M	Oscillator comb frequency spacing
τ	Delay in delay line
μ	Permeability
ω	Magnetostatic surface wave angular frequency
$4\pi M_s$	Saturation Magnetization

AFIT/GE/EE/81D-35

Abstract

This thesis presents an experimental analysis of a magnetostatic surface wave delay line used in a two-four gigahertz feedback loop oscillator. The analysis focused on the multimoding and mode hopping effects. The tuning rate, switching speed and quality factor were also examined.

The results showed that the mode hopping behavior is a result of the interaction of the delay line delay and total loop delay. The multimoding behavior was found to be a function of the loop gain and the delay lines insertion loss, bandpass and delay. Two approaches to help reduce these undesirable effects were outlined.

MAGNETOSTATIC SURFACE WAVE

MICROWAVE OSCILLATOR

I. Introduction

Background

In 1960, Damon and Eshbach theoretically characterized
the existence of two distinct magnetostatic modes on a
ferromagnetic slab.   With the assumption of proper boundary
conditions, their analysis indicated that these modes were
unique, frequency dependent solutions to Maxwell's equations
and the equation of motion of the slab magnetization.   They
determined that as frequency increases beyond the spin wave
region, the magnetostatic behavior changes from one which is
distributed across the volume of the slab to one which is
strictly a surface mode (Ref. 4).

The surface mode has the following characteristics: it
is nonreciprocal; it propagates perpendicular to a magnetic
biasing field;   it is guided by two parallel surface;   the
mode propagates with a velocity between that of acoustic and
light waves;   its velocity is magnetically tunable;   and
most of its energy is concentrated near one surface
(Refs. 4,12).

Later, in 1968, Brundle and Freedman experimentally
excited the magnetostatic surface wave (MSSW) mode on a

thin, single crystal, yttrium-iron-garnet (YIG) slab where the wave lengths of the surface waves were much smaller than the YIG slab dimensions (Ref. 1). Their results closely followed the theoretical mode behavior that was predicted by Damon and Eshbach. The waves were initiated by a single wire that extended across the end face of the slab thus allowing a y-directed surface wave having no z-dependence to propagate.

In 1975, Ganguly and Webb developed a model for excitation of MSSW with microstrip transmission lines (Ref. 6). This model was expanded to include periodic structures by Sethares, Tsai and Koltunov in 1978 (Ref. 12).

Considerable experimental work has been done in several areas of signal processing using magnetostatic wave technology components. Practical tunable MSSW microwave oscillators have been demonstrated by Haworth in 1975 (Ref. 7), Miller and Brown in 1976 (Ref. 8), Castera and Hartemann in 1978 (Refs. 3,4), and Sethares and Stiglitz in 1980 (Ref. 13).

The AFCRL thesis proposal suggested that several parameters of a magnetostatic wave (MSW) delay line oscillator needed to be determined to evaluate its application for Air Force systems. The work would be an extension of the 1980 Sethares and Stiglitz paper and would hopefully explore some of the characteristics that MSW oscillators exhibited.

Statement of the Problem

Until this time, no research had been done on the tuning rate of a MSW delay line oscillator. Frequency modulation and frequency agility characteristics would be important to know for applications in radar and electronic warfare systems. In any oscillator the quality factor and bandwidth are important parameters. These two have not been measured for the delay line oscillators fabricated by Air Force Cambridge Research Laboratory (AFCRL). Previous work has indicated that as the oscillator is tuned in frequency discontinuous jumps occur. Multimoding effects (two or more simultaneous frequencies) can also occur.

Plan of Attack

This thesis concerns itself with the evaluation of the potential of magnetostatic surface wave oscillators for systems application by investigating the following characteristics. First, to determine the bandwidth and quality factor for a MSSW delay-line oscillator provided by AFCRL. Second, to determine the maximum tuning rate and switching speed of the same device. Third, to investigate the mode hopping effect as an oscillator is tuned by the magnetic bias field. Two delay lines will be used in this last experiment. One with 15 aluminum strips of equal width and spacing for the transducers (the same device used in the first two experiments). The other is a device with 15

strips of equal spacing but weighted widths.

Sequence of Presentation

The existing magnetostatic theory for slab geometries and periodic transducers will be discussed first followed by a short discussion of the requirements necessary for oscillation to occur. Next, the experimental schemes for determining the oscillator's three dB noise bandwidth, quality factor, tuning rate and switching speed, and the accompanying results will be presented. This will be followed by an experimental analysis of the multimoding and mode hopping behavior with a possible approach to minimize these two undesirable effects. Finally, a discussion of the results and conclusions drawn from this study will be given.

II. Magnetostatic Theory

Phenomenological Model

Magnetostatic behavior in yttrium-iron-garnet and other similar ferromagnetic materials can be explained by understanding the internal interactions of the crystal magnetic moments as influenced by externally applied fields. There are periodic time-varying RF fields found at the input and the DC biasing field.

In a ferromagnetic material the interaction of the electron spins within the crystal lattice creates a magnetic moment at the ion sites within the structure. The summation of these moments over the total volume yields a total magnetic moment which can be influenced by applied external magnetic fields.

In the simplest case, a single spin, when an external DC field is applied a torque is produced which causes a precession of the magnetic moment about its equilibrium position. The precession rate (a fixed amount) and the precession angle are both functions of the strength of the applied magnetic field, H , and can be expressed as (Ref. 15:5)

$$\omega = \gamma H \tag{1}$$

where γ is the gyromagnetic ratio.

When a RF field (with the same frequency as the precession rate) is added by superposition orthogonal to the DC field the magnetic moment vector will change in two ways. The magnitude of the magnetic moment vector and the precession angle will increase.

When the interaction of the neighboring spins is included an opposing force is created that tends to decrease the magnetic moment vector and the precession angle. This demagnetization, H_d , is a function of the material geometry and can be expressed as follows (Ref. 14:15)

$$H_d = 4\pi M_s N_d \tag{2}$$

with $4\pi M_s$ being the saturation magnetization and N_d the demagnetization factor of the ferromagnetic material. The precessional frequency can now be expressed as

$$\omega = \gamma(H_{DC} - H_d) \tag{3}$$

with H_{DC} = the applied DC field. Remembering that the RF field, H_{RF} , exerts a torque on the spin system, the equation of motion can be expressed as a function of M , the net internal magnetic field, the gyromagnetic ratio, γ , and the applied fields (Ref. 15:60). With

6

$$H_T = H_{DC} + H_{RF} - H_d$$

(4)

$$\frac{d}{dt}\vec{M} = \gamma(\vec{M} \times \vec{H}_T)$$

Many additional factors can be considered that will complicate the analysis of the magnetostatic behavior of the ferromagnetic material. Ionic impurities, crystal lattice dislocations, and surface effects have been ignored. These crystalline imperfections along with temperature have an effect on the spin system. YIG is chosen for MSW devices because its crystalline properties and ease in manufacture make it a model specimen. At present there is not a complete model for all aspects of magnetostatic behavior but the work done by Damon and Eshbach, Brundle and Freedman, Ganguly and Webb, and AFCRL has resulted in fairly good models for at least two types of magnetostatic modes.

Magnetostatic Modes

The two generally accepted and well studied modes are the surface and volume modes. Damon and Eshbach in 1960 developed solutions to Maxwell's Field Equations and the equation of motion of the magnetization for a ferromagnetic slab. The boundary conditions and ferromagnetic slab were considered as shown in Figure 1 (Ref. 5:310).

Because the ferromagnetic material is nonconductive,

7
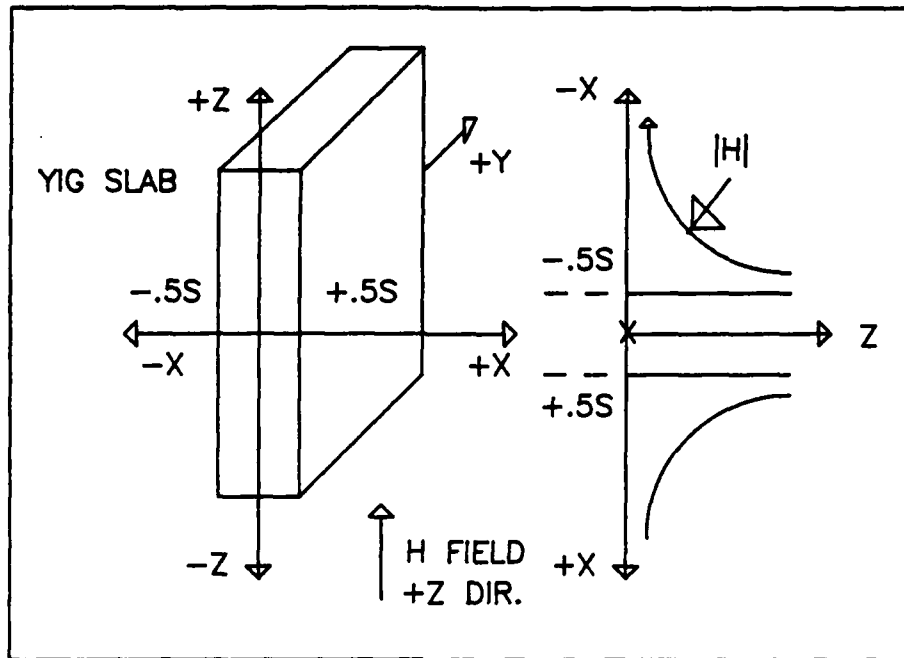
Figure 1. Damon and Eshbach Theoretical Slab and Boundary
Conditions.

Maxwell's equations in the magnetostatic limit become

$$\nabla \times \vec{H} = 0 \qquad\qquad (5)$$

$$\nabla \cdot \vec{B} = 0$$

where

$$\vec{B} = \mu_0 (\vec{H} + 4\pi\vec{M}_s)$$

$$\vec{H} = \vec{H}_{DC} - \vec{H}_d + \vec{H}_{RF}$$

The boundary conditions require that the normal   B   and
tangential H components be continuous at the surfaces   and

that these fields approach zero as x approaches infinity.
The magnetostatic equation of motion presented earlier and
repeated below must be simultaneously satisfied.

$$\frac{d}{dt}\vec{M} = \gamma(\vec{M} \times \vec{H})$$ (4)

Damon and Eshbach found that two frequency dependent
magnetostatic modal solutions exist. The volume mode, or
"bulk effect" mode, occurs when the energy propagation
mechanism is due to spin exchange coupling. The surface
mode, which this thesis is primarily concerned with, occurs
when the energy densities are greatest at one of the slab's
surfaces. The surface wave is a complex phenomenon but its
key characteristics are that its velocity is tunable, it is
nonreciprocal and is dispersive in nature.

The surface wave's dispersion properties can be
characterized by the following equation (Ref. 5:315).

$$r_0{}^2 = r_H{}^2 + r_H + [2 + 2\coth(|k|s)]^{-1}$$ (6)

where

$$r_0 = \frac{\omega}{4\pi M_s \gamma}$$

$$r_H = \frac{H_e}{4\pi M_s}$$

9

k = the MSSW vector number

s = the slab thickness

ω = the MSSW angular velocity

Υ = gyromagnetic ratio

$H_e = H_{DC} - H_d$

The direction of propagation for a surface wave, $\hat{k}$, is determined by the following equation

$$\hat{k} = \frac{\vec{H}_{DC}}{|\vec{H}_{DC}|} \times \hat{n} \qquad (7)$$

where $\hat{n}$ is the surface normal unit vector. Figure 2 shows the relationships of $\vec{H}_{DC}$, $\vec{H}_{RF}$, $\hat{n}$ and $\hat{k}$ as experimentally determined by Brundle and Freedman using single wire transducers for MSSW excitation (Ref. 1,132).

Multistrip Transducer Theory

Magnetostatic wave devices normally make use of microstrips to excite the wave propagation. Ganguly and Webb did a theoretical analysis which described the interaction of a single conducting strip carrying a uniform current with MSSW. In 1978 Sethares, Tsai, and Koltunov expanded this theory to include periodic transducer structures.

The geometry for their analysis is shown in Figure 3. As before we require the simultaneous satisfaction of

10
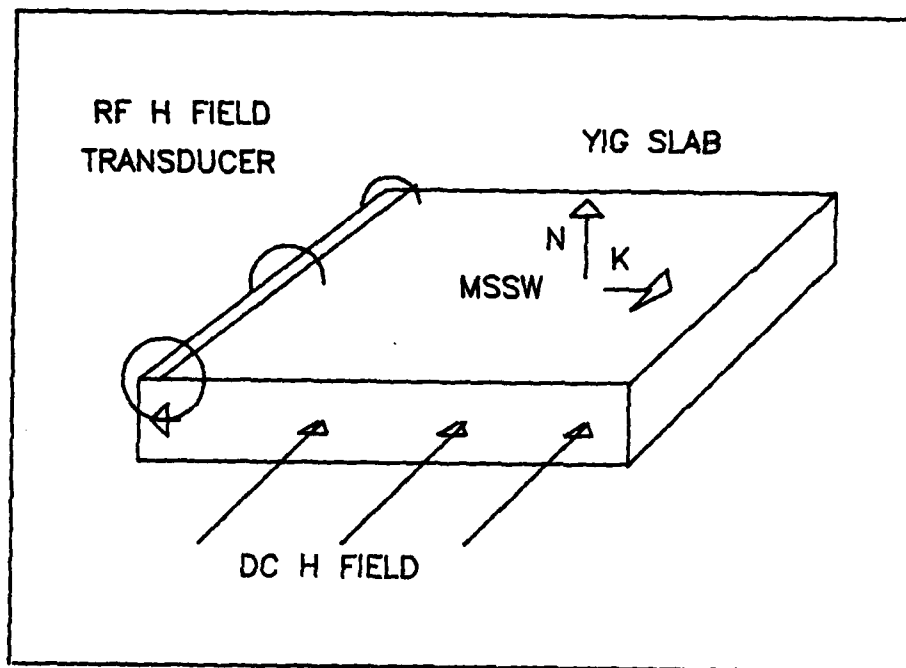
Figure 2. MSSW Propagation Direction, $\vec{k}$, Relative to $\vec{H}_{DC}$ and $\vec{H}_{RF}$.
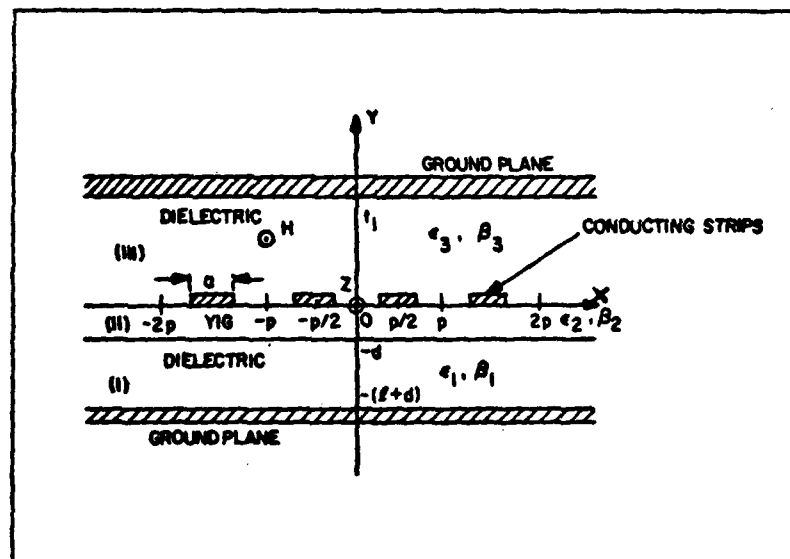
Figure 3. Geometry for the Sethares and Stiglitz System Composed of YIG Film, Conducting Strips, Double Ground Plane and Dielectric Regions.

Maxwell's equations and the gyromagnetic equation. For small signal RF field variations the gyromagnetic equation can be linearized to first order (Ref. 12:9).

$$M_x = \frac{\gamma}{j\omega} (M_s H_y - H_0 M_y) \qquad (8)$$

$$M_y = \frac{-\gamma}{j\omega} (M_s M_x - H_0 M_x)$$

where

$$H_0 = H_{DC} + H_d + H_a$$

$$H_a = \text{anisotrophy field strength}$$

Using $\vec{B} = \mu_0 (\vec{H} + \vec{M})$ with the preceding equations one obtains

$$\begin{bmatrix} B_x \\ B_y \end{bmatrix} = \mu_0 \begin{bmatrix} \mu_{11} + j\mu_{12} \\ -j\mu_{12}\mu_{22} \end{bmatrix} \begin{bmatrix} H_x \\ H_y \end{bmatrix} \qquad (9)$$

Using the appropriate boundary conditions the nonzero fields B_y and H_x were determined. Coefficients were found to be functions of a Fourier Transform of the arbitrary surface current distribution $J(X)$. This was an important result because it provides a procedure for transducer designs. The final forms for B_y and H_x were determined by making the approximation "that in the magnetostatic limit, MSSW wavelengths λ_s are much smaller than the electromagnetic wavelengths λ^0_ε in regions of dielectric constant ε . (Ref. 12;16). This simplifies the following terms for $k_s >> k_\varepsilon^0$.

12

$$\beta \equiv \sqrt{\frac{\mu_{22}}{\mu_{11}}} \qquad s_k = \frac{k}{|k|} = \pm 1 \qquad |k| = k_s \text{ for}$$

<div align="right">surface wave
propagation</div>

$$\alpha_1 = \mu_{11}\beta - \mu_{12}s_k$$

$$\alpha_2 = \mu_{11}\beta + \mu_{12}s_k \tag{10}$$

$$k_\varepsilon^0 \equiv \frac{\sqrt{\varepsilon}\omega}{c}$$

$$k_s = \text{MSSW wave vector number}$$

where

$\mu_{11}, \mu_{12}, \mu_{22}$ are components of the permeability

matrix.

c = speed of light

ω = angular frequency

d, ℓ, and t, are dimensions presented in Figure 3.

can also define

$$T_M \equiv T\big|_{k_s \gg k_\varepsilon^0} = \frac{\alpha_2 + \tanh(|k|\ell)}{\alpha_1 - \tanh(|k|\ell)} \tag{11}$$

and

$$F_{TM}^{(1)}(k,\omega) \equiv \frac{\partial}{\partial k} F_T(k,\omega)\big|_{k_s \gg k_\varepsilon^0} \tag{12}$$

$$= s_k \Big\{ t_1(\alpha_1 T_M - \alpha_2 \exp[-2\beta|k|d]) \text{csch}^2(|k|t_1)$$

13

$$+ 2d\beta(1-\alpha_2\coth(|k|t_1)\exp[-2\beta|k|d])$$

$$- \frac{2\mu_{11}\beta\ell[\alpha_2\coth(|k|t_1)+1]\mathrm{sech}^2(|k|\ell)}{[\alpha_1-\tanh(|k|\ell)]^2}\Bigg\} \tag{12}$$

their final equations for the MSSW's in either direction $(s_k = \pm 1)$ were as follows:

Region 1.

$$B_y{}^{(s)} = - s_k\mu_0 G(T_M+1)\left[\frac{\sinh[|k|(y+d+\ell)]}{\cosh(|k|\ell)}\right]$$

$$\tag{13}$$

$$H_x{}^{(s)} = jG(T_M + 1)\left[\frac{\cosh[|k|(y+d+\ell)]}{\cosh(|k|\ell)}\right]$$

Region 2.

$$B_y{}^{(s)} = - s_k\mu_0 G\left[\frac{\alpha_1 T_M\exp[\beta|k|(y+d)]}{} -\alpha_2\exp[-\beta|k|(y+d)]\right]$$

$$\tag{14}$$

$$H_x{}^{(s)} = jG[T_M\exp[\beta|k|(y+d)]+\exp[-\beta|k|(y+d)]]$$

Region 3.

$$B_y{}^{(s)} = - s_k\mu_0 G[\alpha_1 T_M\exp[\beta|k|d]-\alpha_2\exp[-\beta|k|d]]$$

$$\left|\frac{\sinh[|k|(t_1-y)]}{\sinh[|k|t_1]}\right| \tag{15}$$

14

$$H_x^{(s)} = -jG[\alpha_1 T_M \exp[\beta|k|d] - \alpha_2 \exp[-\beta|k|d]]$$

$$\left\{ \frac{\cos[|k|(t_1 - y)]}{\sinh[|k|t_1]} \right\} \tag{15}$$

where

$$G = \frac{\mathfrak{J}(k)\exp[-\beta|k|d]}{F_{TM}^{(1)}(k,\omega)} \tag{16}$$

and

$$\mathfrak{J}(k) = \int_{-\infty}^{\infty} J(x)\exp[jkx]dx$$

It is also understood that the term $\exp[j(\omega t - kx)]$ is present in equations 13-15.

Conditions for Oscillation

Two conditions, gain and phase, must be met for oscillation to occur in a feedback delay line oscillator. The amplifier gain must exceed the feedback loop's components losses for oscillation to occur. The phase must satisfy the following condition for oscillation to occur (Ref. 13:2274).

$$2\pi f_0(\tau + t_0) = 2\pi n \qquad (17)$$

where

f_0 = frequency of oscillation

τ = the delay found in the delay line

t_0 = additional delay for the electrical components

n = 1,2,3,...

Several simultaneous frequencies can be present when equation 17 is satisfied for more than one value of n and sufficient gain is available. The spacing between these frequencies, comb frequency spacing (Δf_M), can be determined by equation 18.

$$\Delta f_M = \frac{1}{\tau + t_0} \qquad (18)$$

III. Experimental Procedures and Results

Delay Line Parameters

The first delay line provided by AFCRL was fabricated using yttrium-iron-garnet placed on two narrow band multielement transducers. Each consisted of 15 aluminum strips in the form of a grating. Each strip was three microns (μm) thick, one centimeter long, 178 μm wide, adjacent strips were spaced 300 μm between center. The second delay line was identical to the first except the 15 strips were weighted (different widths). The widest element was 338 μm and the narrowest 58 μm . Each adjacent strip was incremented by 40 μm . The widest strip was the middle of the 15 strips (Ref. 13,2273).

Delay Line Oscillator Components

A DC electromagnet was used to provide the DC bias field. In combination with a variable DC power supply an uniform field could be generated over a linear range from zero to 1200 gauss. The resultant field, measured between the pole pieces, versus applied current is shown in Figure 4. Maximum current output available was five amps and the magnets DC resistance was 33 ohms. The magnet has three inch diameter pole pieces spaced 2-3/4 inches apart. The delay line fits within the pole pieces in a region where a uniform field is present.

17

FIELD STRENGTH (GAUSS)

SLOPE ≈ 520 GAUSS/AMP

CURRENT (AMPS)
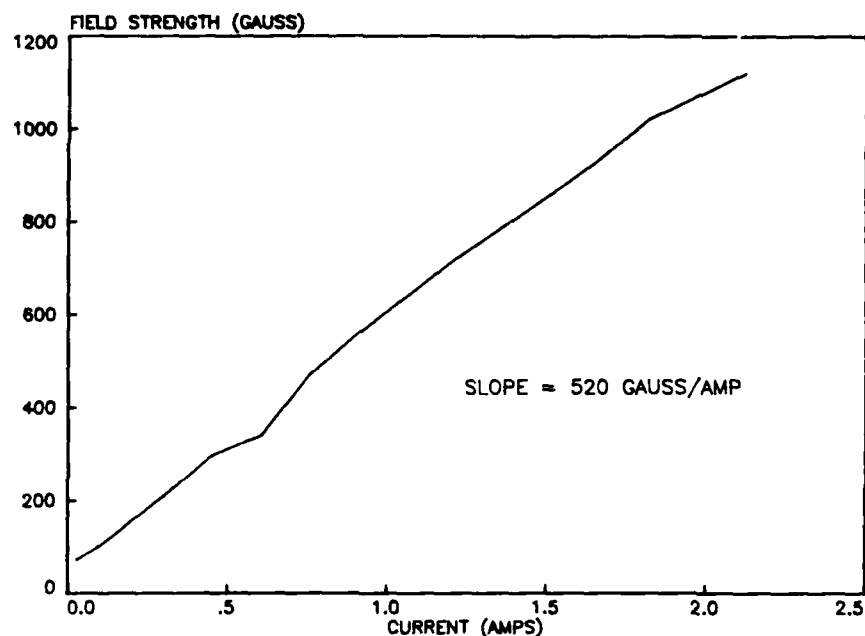
Figure 4. Magnetic Field Strength versus Applied Current.

The components were arranged in a feedback loop as indicated in Figure 5. Two amplifiers operated in cascade were necessary to provide the necessary gain. A variable attenuator and variable phase shifter was included to adjust the gain and phase conditions for oscillation as needed. A ten dB directional coupler was used to provide an output to the spectrum analyzer. Figure 6 shows the parameters of the loop components.

Measuring Delay Line Insertion Loss

Using a sweep oscillator as a signal source the bandpass for both delay lines was determined with a spectrum analyzer. Figure 7 shows the bandpass for the unweighted

18
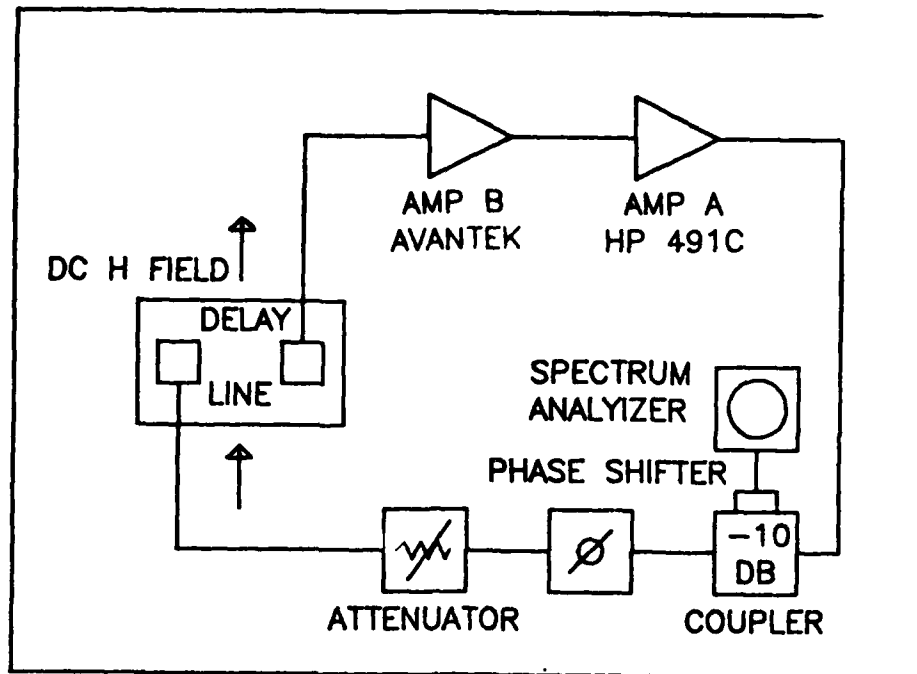
Figure 5. Delay Line Oscillator Equipment Configuration.

transducer case for a bias field of 525 gauss with a center
frequency of 2920 MHZ and a corresponding insertion loss
(IL) of 30 dB . Figure 8 shows the bandpass for the
weighted transducer case for a bias field of 460 gauss.
Several peaks are present separated by approximately 16.5
MHZ . The lowest IL, 27 dB , occurred at 2897 MHZ . Figure
9 shows a comparison of the two transducers with the bias
field adjusted so the peak IL occurs at 2477 MHZ .

Also present on this graph is the value of the
available gain in the loop. It illustrates that for those
frequencies where the gain exceeds IL that oscillation could
occur. It is obvious that, depending on the phase
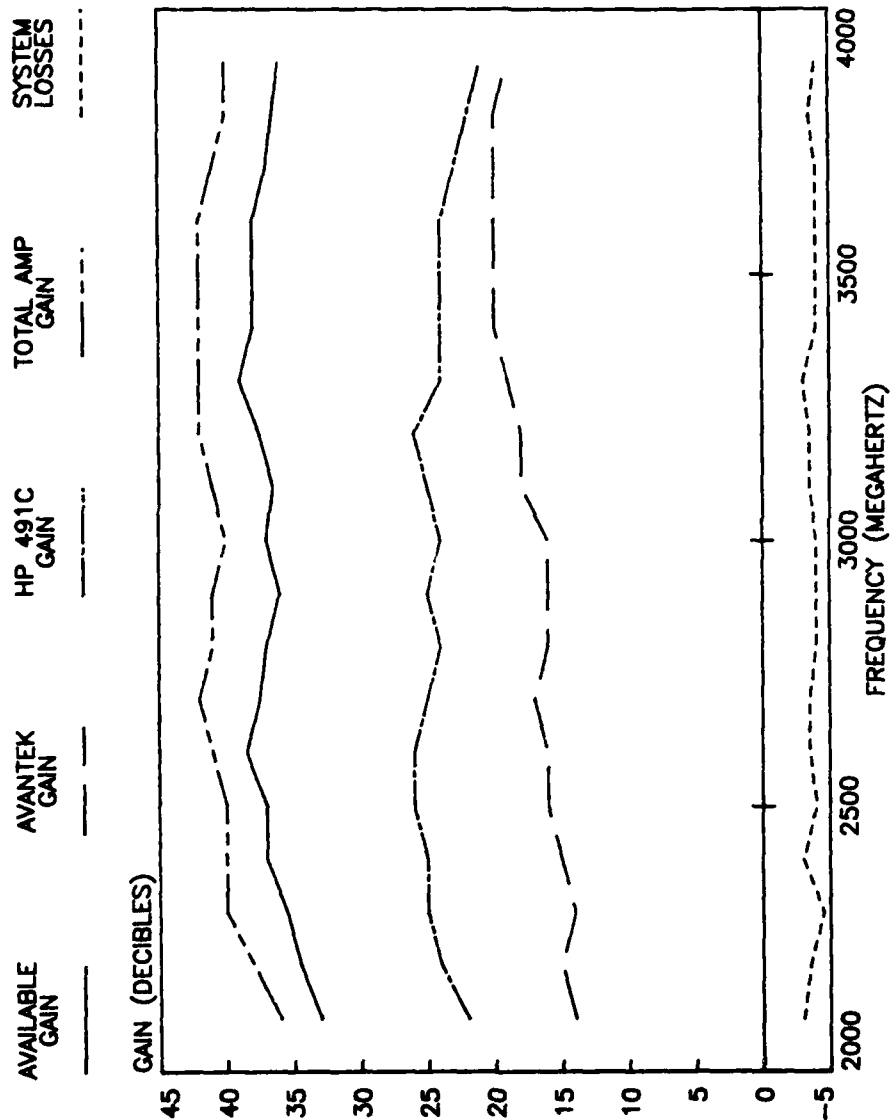
LOSSES INCLUDE: Phase Shifter, Coupler, Cables, and Attenuator.

Figure 6. Amplifier Performance and System Losses.

20
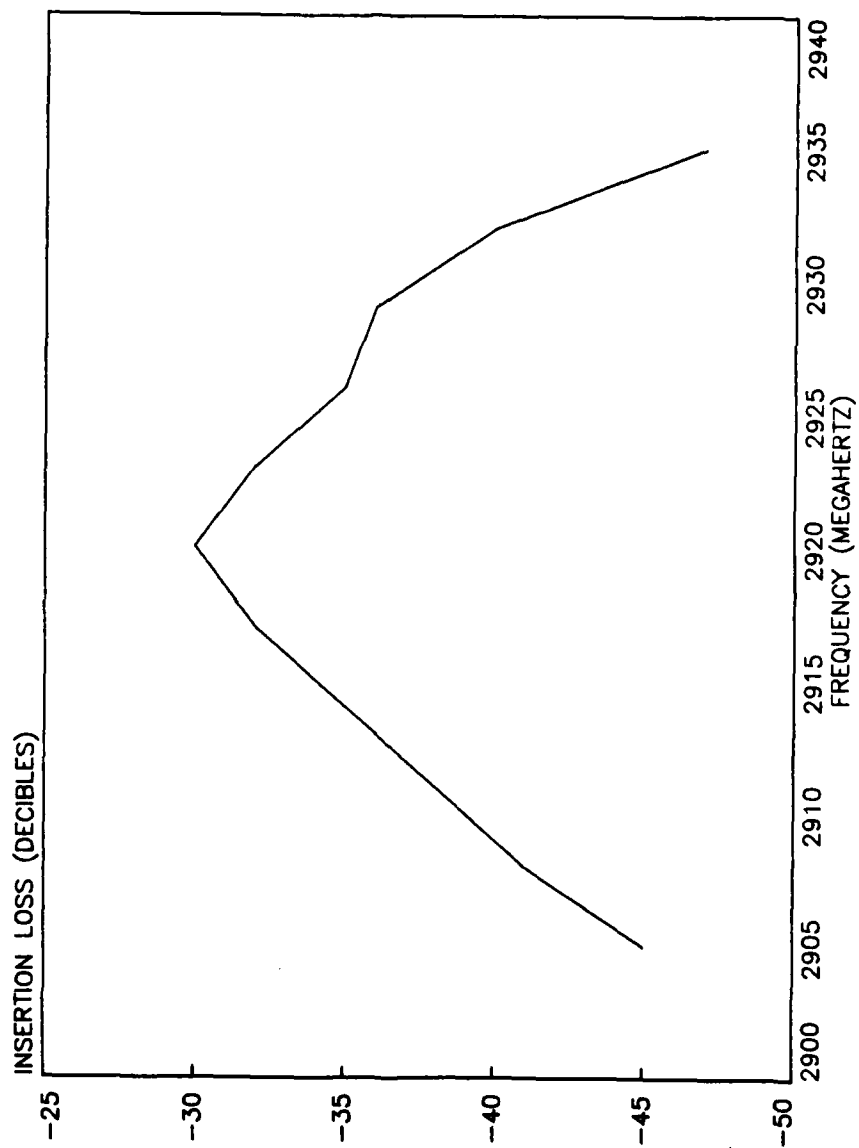
Figure 7. Bandpass for Unweighted Delay Line with a 525 Gauss Bias Field.
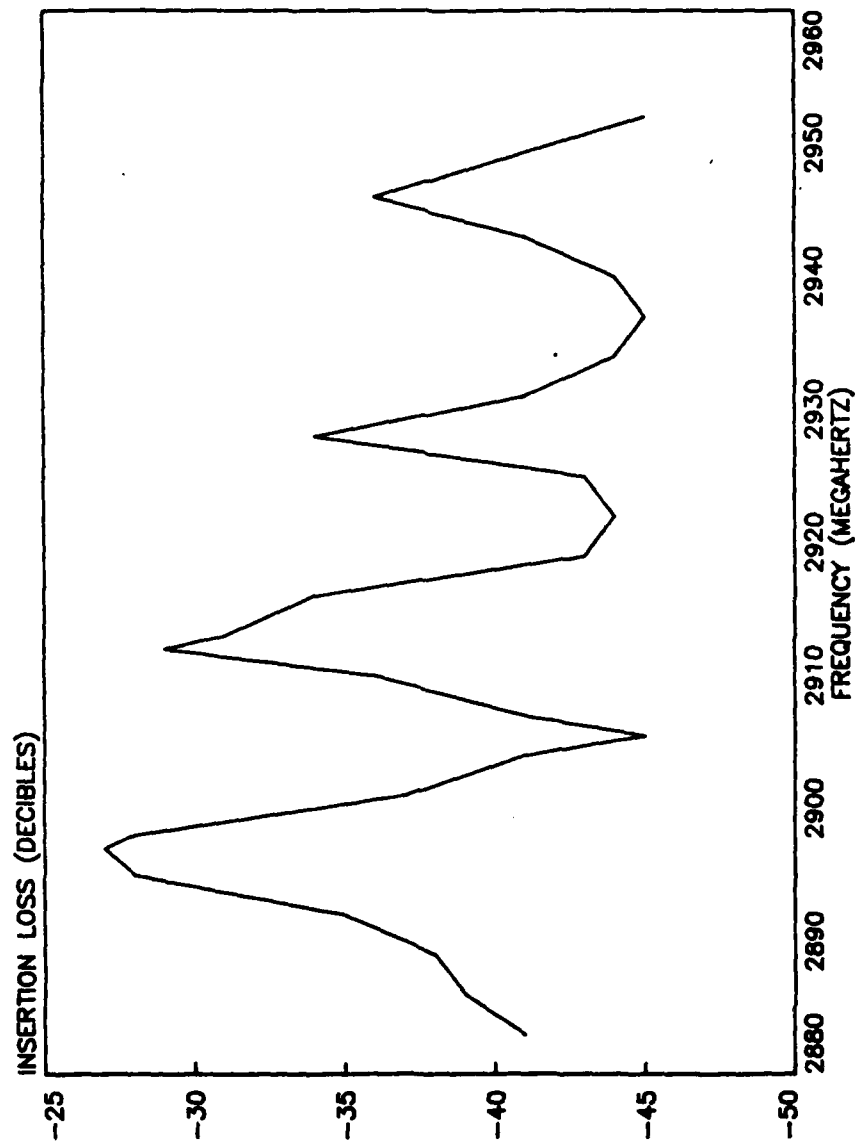
Figure 8. Bandpass for Weighted Delay Line
with a 460 Gauss Bias Field.

22
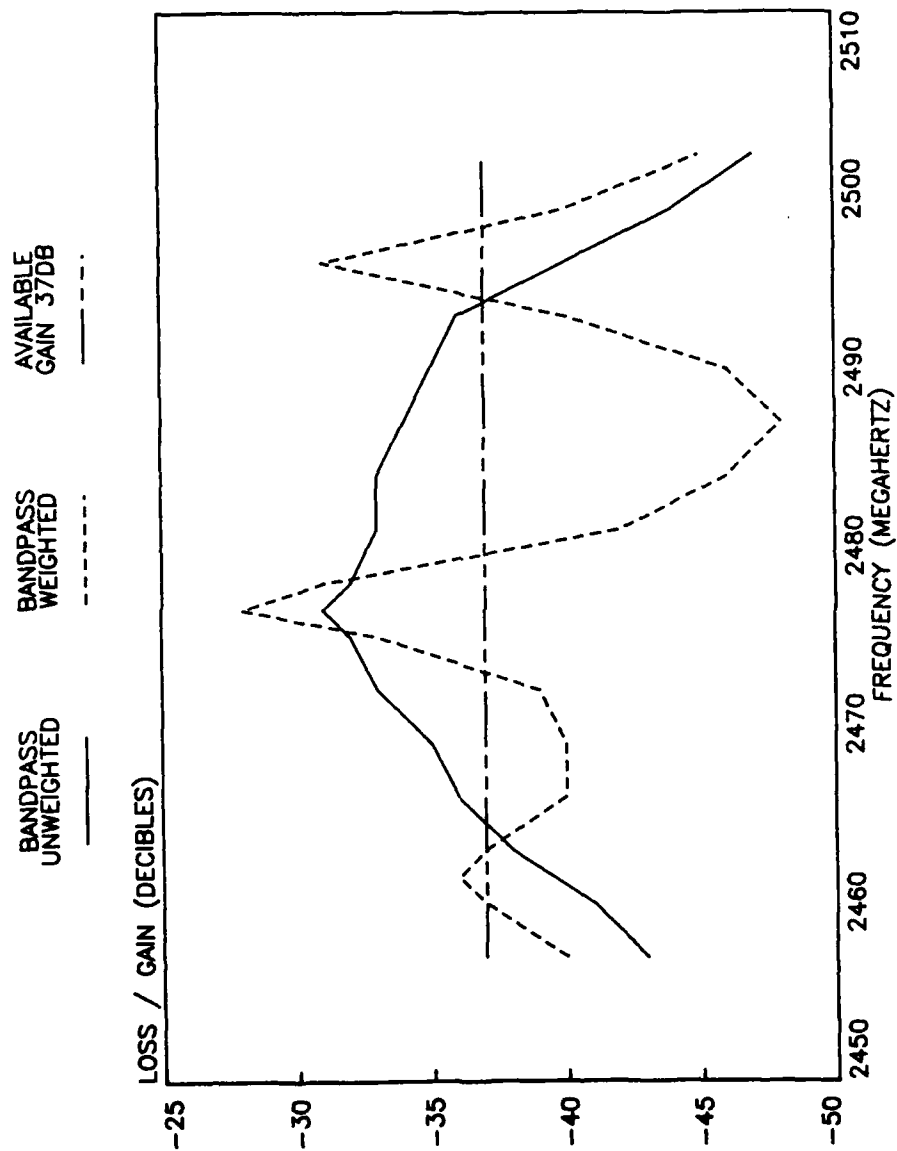
Figure 9. Comparison of Delay Line Bandpass with a Common Center Frequency.

condition, the possible oscillator frequencies could be different for the two transducer cases.

Figure 10 shows the best insertion loss for a particular frequency for the unweighted and weighted transducer delay lines. This data was obtained by measuring the delay line bandpass for many different bias field strengths. For all frequencies the weighted case had the lower insertion loss. Again the available gain is plotted to illustrate the range of frequencies that the gain condition is satisfied. For the first case oscillation is possible from approximately 2200 MHZ to 3700 MHZ . For the second case the gain condition is always satisfied.

Measuring Oscillator Frequency versus Bias Field

The delay line oscillator can be tuned in frequency by varying the DC bias Field. Discontinuous jumps occurred for both delay lines. Regions of simultaneous frequencies also occurred for both cases. Figures 11 and 12 show how the oscillator frequency varied for the unweighted case. Figures 13 and 14 show similar results for the weighted case, first with 37 dB of available gain and the second case with three dB attenuation. Clearly, the two devices behaved differently when used as oscillators. This behavior will be examined more in detail in a latter part of this section. The results do correspond well to that predicted by the gain versus IL graphs and the results presented by Sethares and Stiglitz.
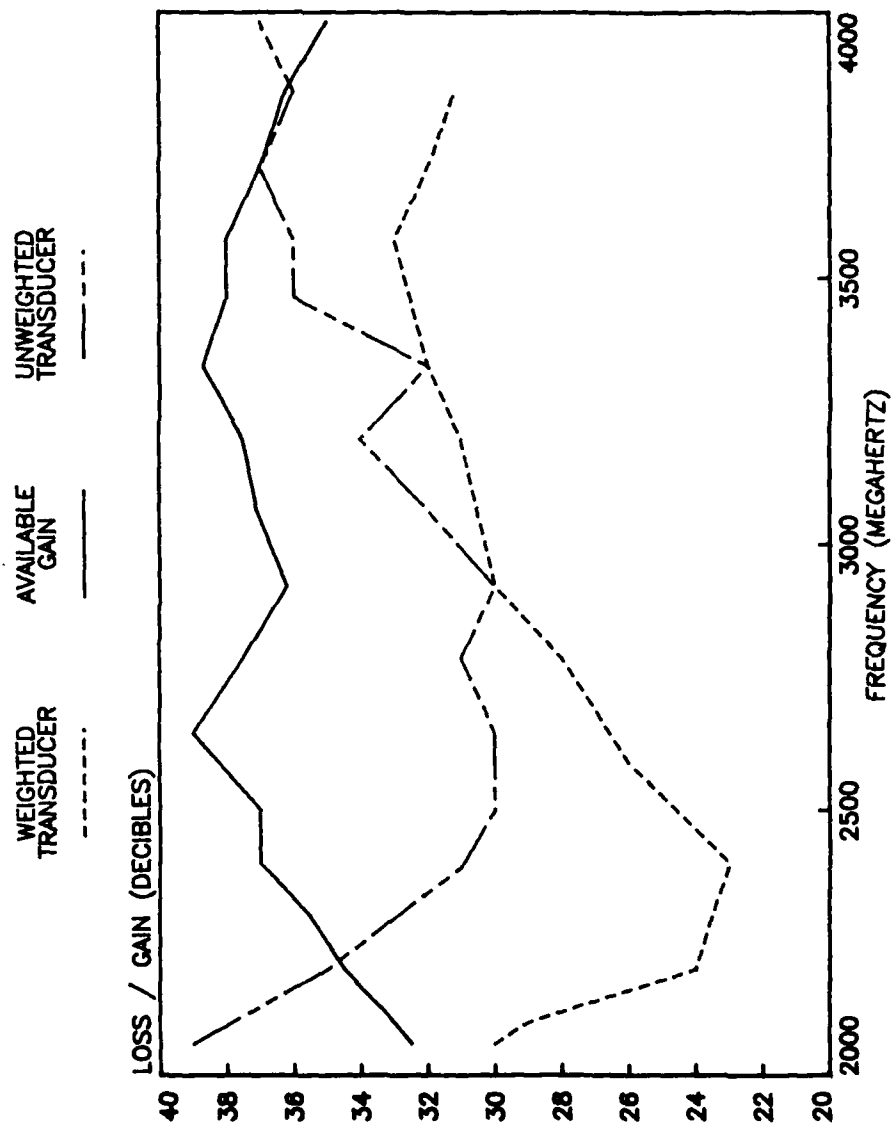
Figure 10. Insertion Loss for Both Delay Lines Compared with Available Gain.
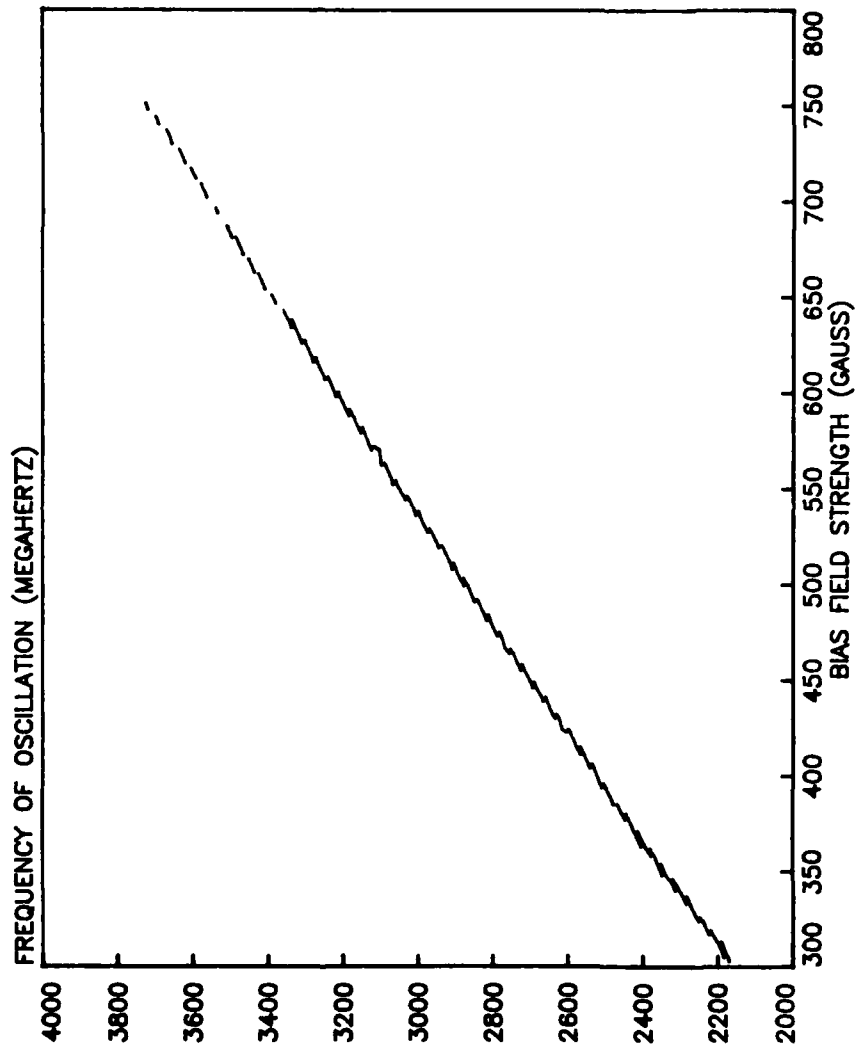
Figure 11. Oscillator Frequency Versus Bias Field
Strength for Unweighted Case.

26
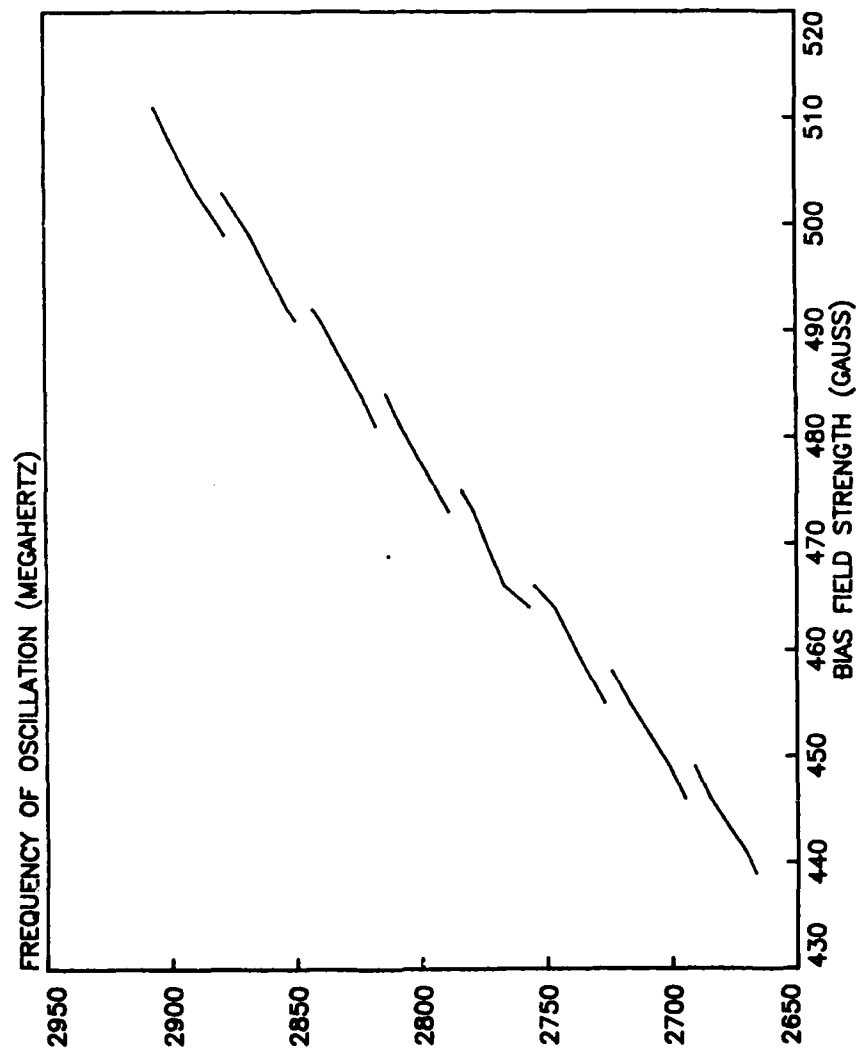
Figure 12.   An Expansion of Previous Chart Showing
Multimoding and Mode Hopping Effects.

27
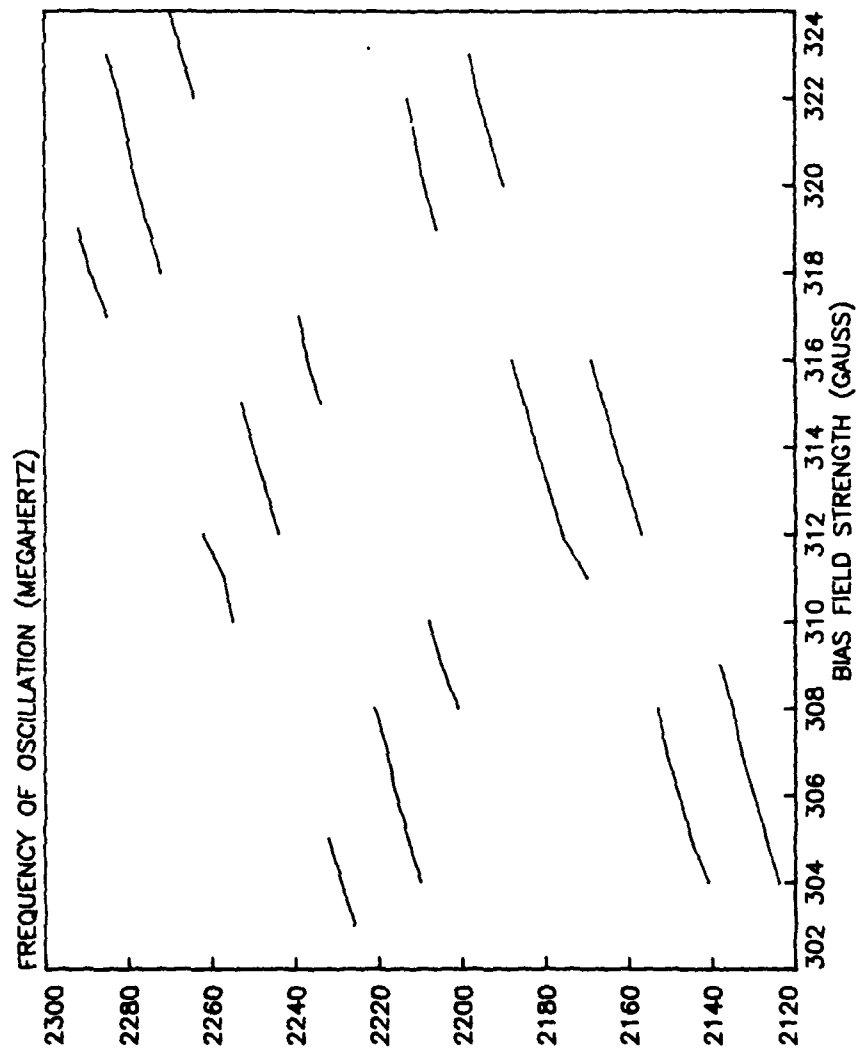
Figure 13. Oscillator Frequency Versus Bias Field Strength for the Weighted Case over a Fraction of the Tuning Region.

28
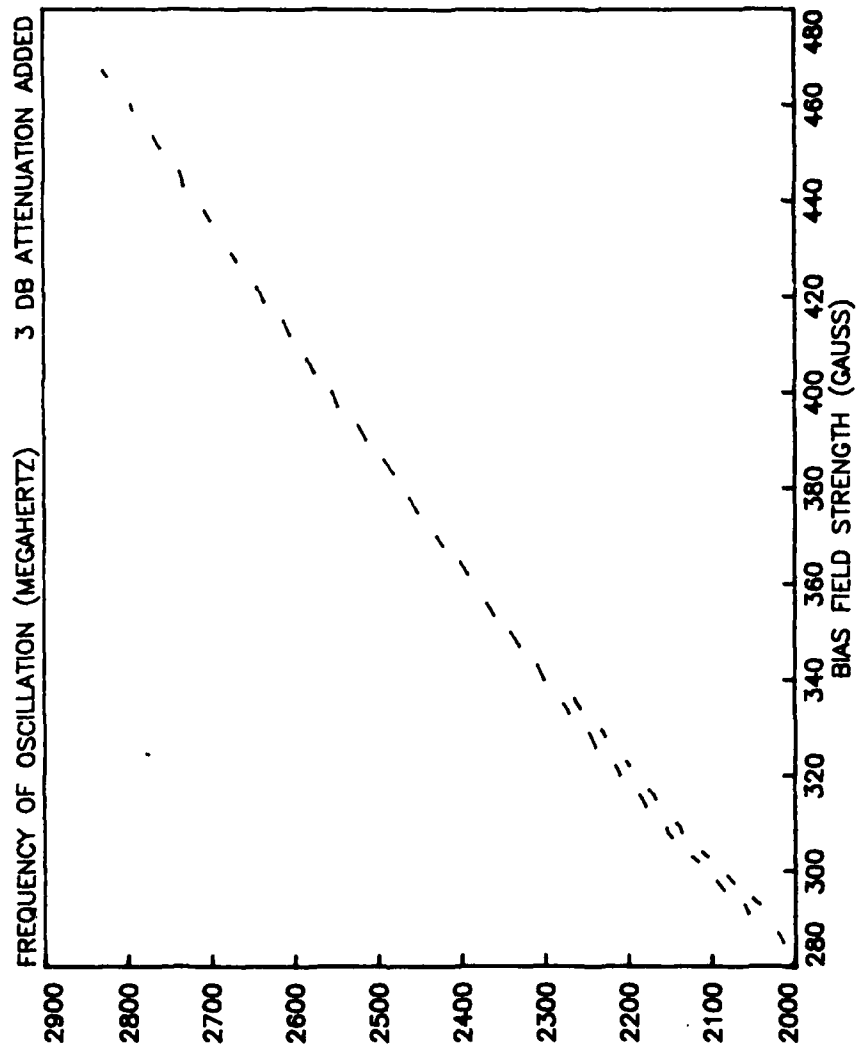
Figure 14. Oscillator Frequency Versus Bias Field Strength for the Weighted Case over the Full Tuning Region (additional attenuation).

Oscillator Noise Bandwidth and Quality Factor

For any oscillator the three dB noise bandwidth, BW_3 , and quality factor, Q , are important measures. The noise bandwidth of the delay line oscillator was measured at five points between two and four GHZ . At each frequency the feedback gain was adjusted for a gain/loss ratio of approximately one. The quality factor was also calculated using the following relationship (Ref. 2:384).

$$Q = \frac{f_0}{BW_3} \qquad (19)$$

where f_0 = frequency of oscillation. The measured values for BW_3 and the calculated ones for Q are presented in Table I and Figure 15. Figure 16 shows the spectrum analyzer display with f_0 = 2.998MHZ . In contrast to crystal oscillators, the noise bandwidth was found to be relatively constant. This behavior is best explained by examining the individual components of the total Q . The total Q of a MSSW delay line oscillator or resonator is affected by external factors such as the transducer effects and YIG slab end reflections, Q_{ext} , the array factor, Q_r , (primarily associated with MSSW resonators), and the material loss, Q_m . The total Q_T is

$$\frac{1}{Q_T} = \frac{1}{Q_r} + \frac{1}{Q_m} + \frac{1}{Q_{ext}} \qquad (20)$$

30

TABLE I		
3 DB Noise Bandwidth and Quality Factor		
Frequency of Oscillation (MHz)	3 dB Noise Bandwidth (MHz)	Quality Factor
2090	1.62	1290
2500	1.62	1543
2998	1.59	1885
3500	1.65	2121
3898	1.62	2406
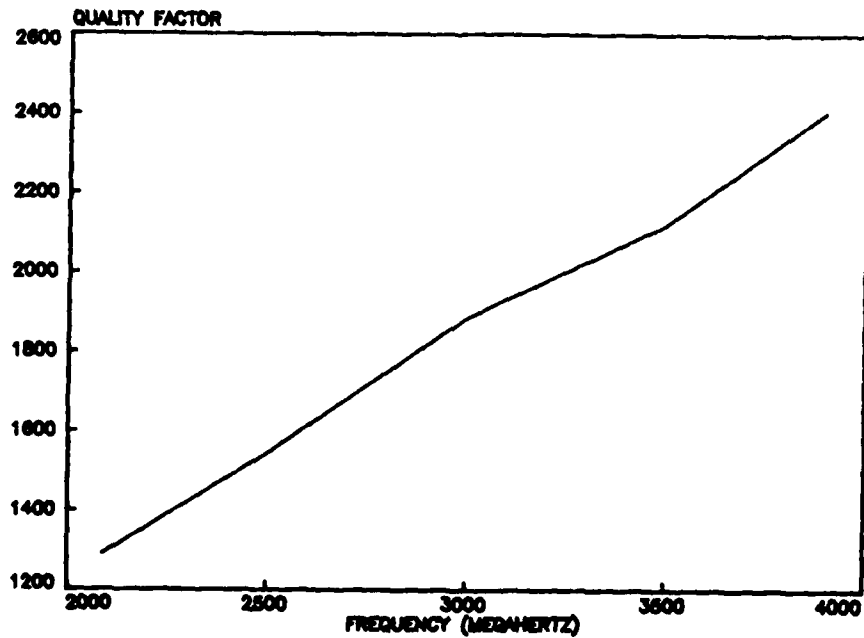
Figure 15. Quality Factor versus Frequency.

31

HOR — 0.3 MHZ/DIV   VERT — 2 DB/DIV
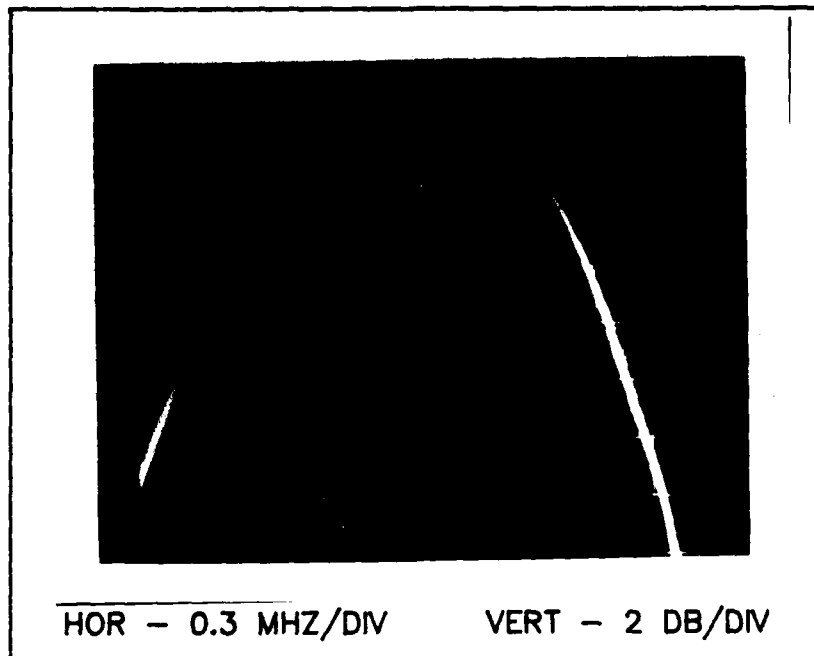
Figure 16.   Spectrum Analyzer Display of a Single Oscillator
              Mode at 2998 MHZ.

In a quartz oscillator Q_m becomes the dominant factor as frequency is increased. In a MSSW delay line oscillator the transducer effects, which are relatively frequency independent, are dominant. The transducer effects of interest are the degree of coupling to the YIG film by both input and output transducers and the amount of loss found in the transducers (Ref. 2:384).

Tuning Sensitivity

The shift in oscillator frequency for a given change iñ bias field strength can be determined by measuring the slopes of the individual lines plotted in Figures 11 and 14.

For the unweighted transducer delay line the average slope for the 51 continuous tuning regions between 2.1 GHZ and 3.8 GHZ was 2.42 MHZ per gauss. The overall slope of the lines was 3.48 MHZ per gauss. Similarly, for the weighted transducer delay line oscillator the average slope was 3.40 MHZ per gauss and the ratio was .766.

It will be shown in the multimoding part of this section how the position and magnitude of the delays found in the feedback loop create this dual slope behavior. The ratios presented will be confirmed using a different experimental procedure and the difference in the ratios for the two transducer cases will be shown to be a result of the difference in the device's delay.

Tuning Rate and Switching Speed

For the purposes of this study the tuning rate of the oscillator is defined as the speed the oscillator can be tuned continuously from one frequency to another. The switching speed is how fast the oscillator jumps from one frequency to another. Both are important parameters for an oscillator that could have application in radar or electronic warfare systems.

Knowing the tuning sensitivity for unweighted transducer delay line is approximately 2.5 MHZ/gauss, it was necessary to modulate the bias field by one or two gauss. Coils were wound around both DC electromagnet pole pieces to effect a

change in the bias field from the quiescent state. The coils were powered by a pulse generator and power amplifier combination/. The coils were wound on the DC magnet's pole pieces with #32 magnet wire. Their DC resistance was 1.6 ohms per each ten turns. Their physical arrangement is shown in Figure 17. The inductance, L , is given by (Ref 11:311)

$$L = N^2 a\mu[\ln\left(\frac{16a}{d}\right) -2]\qquad(21)$$

where

    N = number of turns in coil

    a = radius of pole piece

    μ = permeability of the steel

    d = diameter of wire = .274 mm

The number of turns was varied to provide different field strengths and rise times. A square wave was used for the switching speed and a sine wave was selected for the tuning rate measurements.

The switching speed was calculated by dividing the shift in frequency by the time it takes for the current in the small coils to change from one value to another. The rise time and current values were measured using an oscilloscope that was across a one ohm resister in series with the coils. The assumption was made that for a given

34

```
         30 TURNS WOUND ON EACH POLE PIECE

      →| .9 |←——— 8.35 ——————→| .9 |←

   M  ┌──┬────┐                    ┌────┬──┐  M
   A  │  │////│             ↑      │////│  │  A
   G  │  │////│            3.81    │////│  │  G
   N ─│──│////│── — — — — — ─│─────│////│──│─ N
   E  │  │////│            3.81    │////│  │  E
   T  │  │////│             ↓      │////│  │  T
      └──┴────┘                    └────┴──┘
   COIL 1 |←——— 6.35 ————————→| COIL 2

         GAUSS METER PROBE AT CENTER
         ALL DIMENSIONS IN CENTIMETERS
```
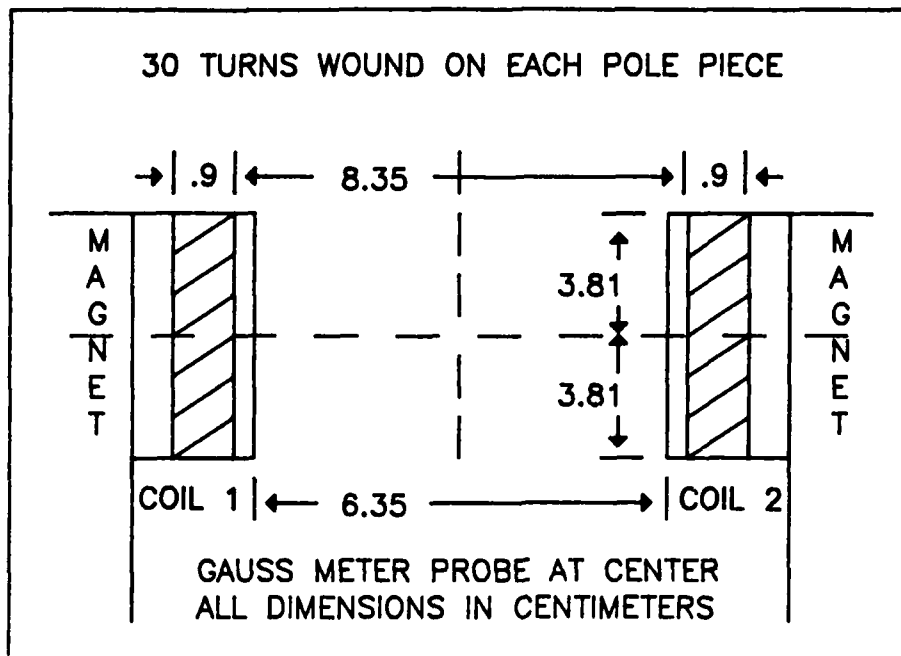
Figure 17. Incremental Coil Placement Diagram.

current a corresponding field and oscillator frequency
existed.   The gauss meter used had an output for measuring
AC fields that was displayed on a dual trace oscilloscope
along   with the coil currents.   This output was   available
for AC fields up to 400 hertz.   The scope display showed
that up to this limit the field strength followed in phase
with the coil currents.   Figure 18 shows the scope display
with the field strength on the top trace and the coil
current on the bottom for a square wave with a period,
T=.05 secs, and peak to peak deflection of 400 milliamps
(ma).

     A slow pulse train,   T=1 secs, was selected for the

```
TOP—FIELD STRENGTH        BOTTOM—CURRENT
```

```
HOR — 5 MSEC/DIV      VERT — 0.1V/DIV
```
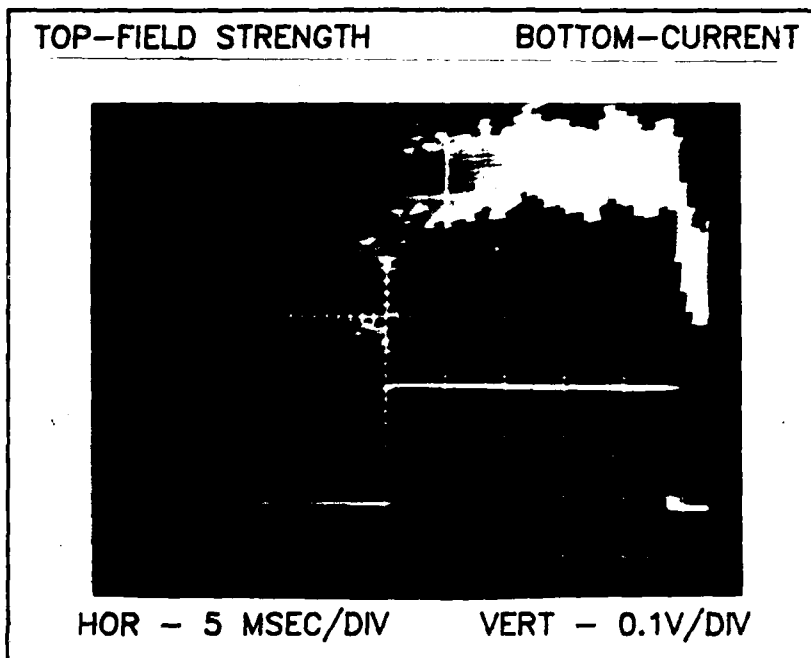
Figure   18.   Oscilloscope Display Showing   Incremental
                  Magnetic Field Strength and Coil Current.

switching speed measurements to allow ease in measuring the

change in gauss and frequency.   This also meant that the

rise time for the current was a small part of the period.

Table II shows the values obtained for the frequency shift,

coil current, switching time, field strength change and

switching speed.   The DC bias field was set at 380 gauss

with an original oscillator frequency of 2800 MHZ.   Figure

19 shows the spectrum analyzer display for the 20 turn case

with a current of 200 milliamps (ma).

     The   fastest   switching speed observed was   .1824

MHZ/microseconds (μsec) . This is considerably slower than

the   ten   MHZ/μsec switching speed Tsai and   Sethares

36

TABLE II
Determination of Switching Speed

Coil Size (turns) #	Step Change in Field and Current applied (gauss & milliamps)	Frequency Shift (MHz)	Switching Time ~ (μsec)	Switching Speed (MHz/μs)
10	+/- .4 & 200	+/- 1.0	28	.0714
10	.8 600 *	1.8	30	.1200
10/10	.6 200	1.6	90	.0356
30/0	1.1 200	3.0	120	.0500
30/10	1.5 200	4.5	100	.0900
30/10	3.0 450 *	7.0	105	.1334
30/30	2.4 200	6.0	160	.0750
60/30	3.7 430 *	15.5	170	.1824

NOTE: # The number of turns on coil 1 / coil 2.
* Maximum allowable current without pulse distortion.
~ Time to change 90% of total current swing.

HOR — 1 MHZ/DIV   VERT — 5 DB/DIV
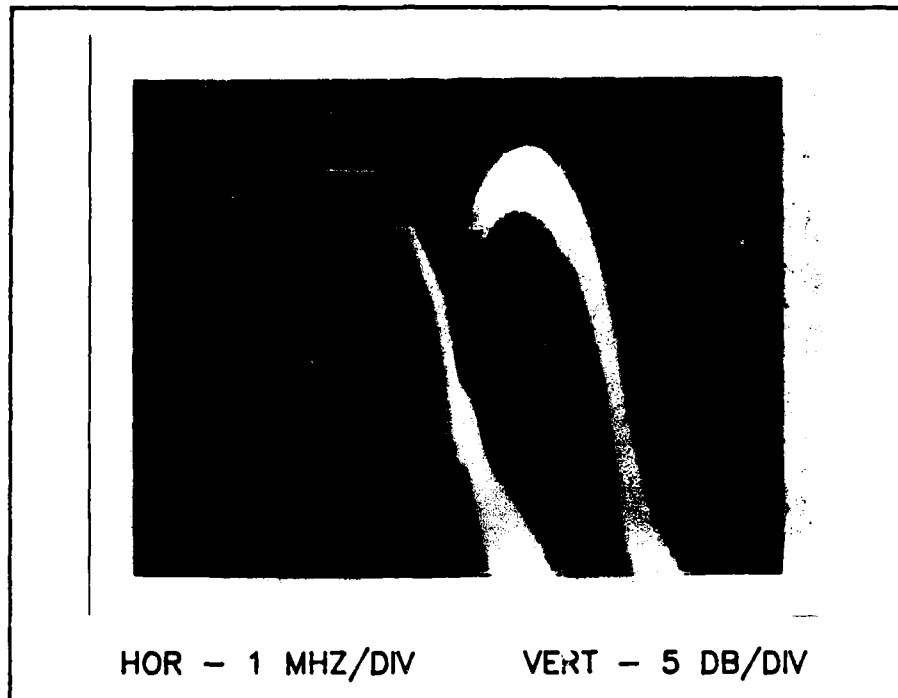
Figure 19.   Spectrum Analyzer Display Showing the Effect of
              200 ma Square Wave in Two Ten Turn Coils.

determined for a MSSW band stop filter (Ref. 16,2273).   The
0.1824 MHZ/μsec result may not be the upper limit of the
device.   Either a coil with a shorter rise time and larger
induced frequency shift needs to be built or a different
experimental setup needs to be developed.

The   tuning   rate was determined with   the   same
experimental setup except a sine wave was used.   The limit
occurs when the oscillator frequency will not change as fast
as the modulating H field changes.   Table III shows the
values measured using two ten turn coils and an AC current
with a peak value of 200 ma .   Figure 20 shows the spectrum
analyzer displaying several AC current frequencies.

38

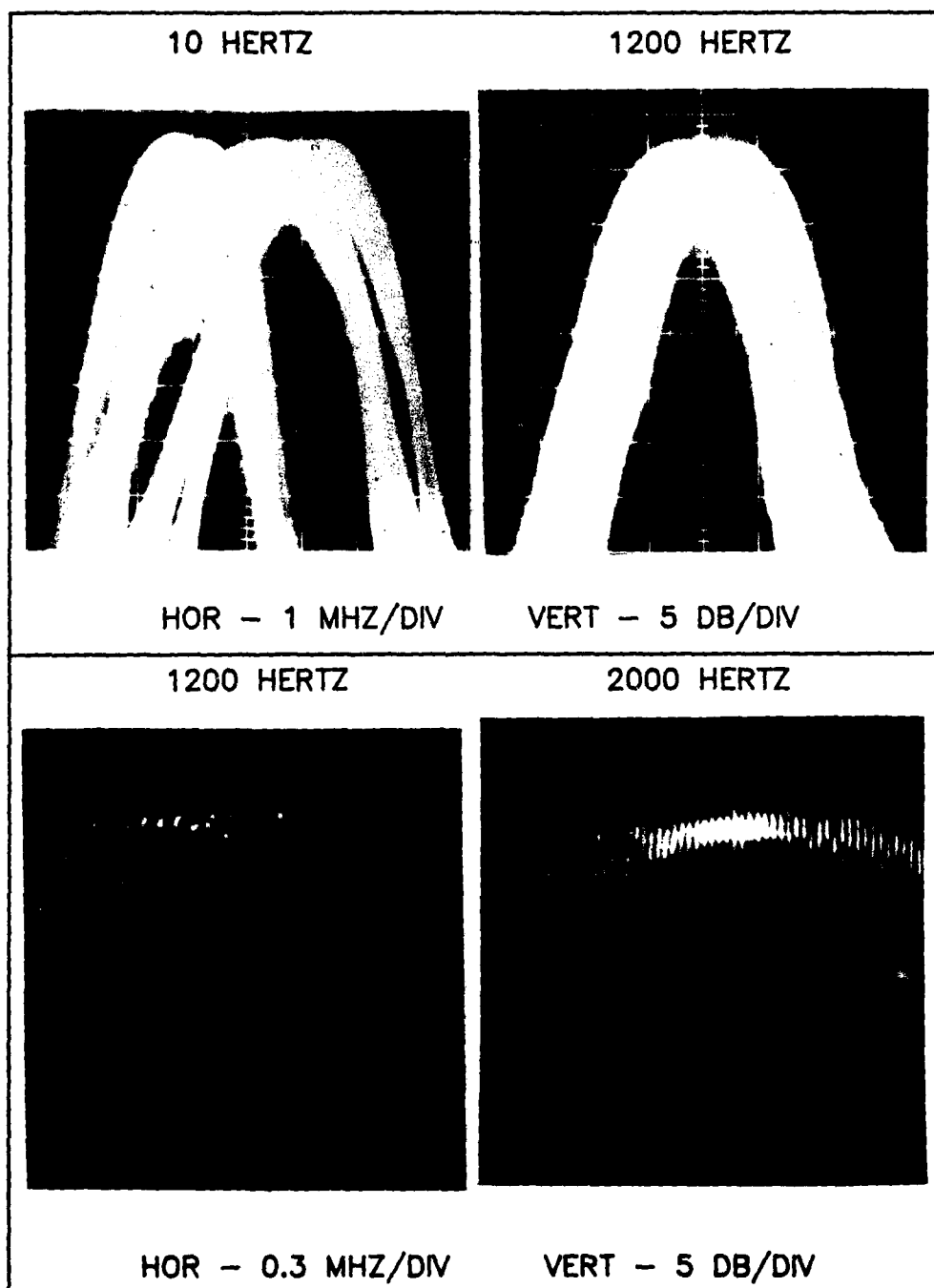| TABLE III Determination of Tuning Rate		
AC Current Frequency (Hertz)	Frequency Shift (MHz)	Tuning Rate (MHz/sec)
.1	4.2	.84
10	3.9	78
20	3.8	152
40	3.6	288
60	3.4	408
80	3.2	512
100	3.1	620
200	2.7	1080
300	2.5	1500
400	2.3	1840
500	2.2	2200
600	2.0	2400
700	1.8	2520
800	1.7	2720
900	1.6	2880
1000	1.5	3000
1100	1.4	3080
1200	1.3	3120
1300	1.2	3120
1400	1.1	3080
1500	0.9	2700
2000	0.6	2400

Figure 20. Spectrum Analyzer Displays Showing Effect of 200 ma Sine Waves In Two Ten Turn Coils.

The peak tuning rate occurred between 1200 and 1300 HZ at approximately 3120 MHZ/sec. This is roughly 60 times slower than the switching speed previously determined. Considering the tuning rate requires a continuous change in frequency whereas the switching speed is a discontinuous change this is an acceptable result.

Multimoding and Mode Hopping

Relating back to Figures 12 and 13, the multimoding and mode hopping effects were clearly seen. When two or more frequencies existed the available gain was such that sufficient delay line bandpass existed for the phase condition to be satisfied for more than one frequency. As shown by Equation 18 below, the spacing was a function of the total delay in the feedback loop.

$$\Delta f_M = \frac{1}{\tau + t_0} \tag{18}$$

For the unweighted case Δf_M was ten MHZ, therefore $\tau + t_0 = 100$ nanoseconds (nsec). The delay line bandpass had only one peak value and was somewhat flat over ten to 15 MHZ. This allowed the gain condition to determine the region of continuous tuning and the presense of any additional frequencies.

In the weighted case the delay line bandpass had several peaks of about the same IL that selected from those

frequencies that had met the phase condition. The separation between adjacent peaks was about 16.5 MHZ. Assuming the total delay from one delay line to another did not differ too much on the basis of the weighting of the transducers, we would expect a Δf_M of around ten MHZ.

The data plotted in Figure 14 showed that the spacing was 17.5 MHZ, therefore the real Δf_M would be 17.5/2 = 8.75 MHZ. This means the total delay is 113.6 nsecs, which is fairly close to the 100 nsec value for the other delay line. If the lines plotted on Figure 13 were continued past the break, the distance from one line to another would be about nine MHZ .

The question presented by AFCRL to me was what causes the oscillator to jump from one set of frequencies to an adjacent set? Castera attributed the behavior to "the difference between the variation of the oscillator frequency and that of the delay line frequency response versus magnetic field" (Ref. 3,827).

The following relationship would then hold true

$$\frac{\Delta f}{\Delta f_{BP}} = \frac{\tau}{\tau + t_0} \qquad (22)$$

where

Δf_0 = change in oscillator frequency for a given bias field.

Δf_{BP} = change in peak delay line bandpass value for the same field bias.

42

τ = delay in delay line.

t_0 = electrical components delay.

This relationship says that the delay line bandpass moves faster than the phase condition as the bias field is increased. This behavior is due to the presense of t_0 in the oscillator term but not in the delay line term.

The value for t_0 was measured by replacing the delay line by a fixed attenuator and recording the oscillator frequencies. The values for the individual components were:

$$
\begin{array}{rl}
\text{AMP A} & 23.7 \text{ nsec} \\
\text{B} & 2.4 \\
\text{Remaining Loop Components} & \underline{6.2} \\
t_0 = & 32.3 \text{ nsecs}
\end{array}
$$

This meant τ for the unweighted transducer delay line was 67.7 nsecs and for the weighted case 81.3 nsecs. The ratio of τ to $t+t_0$ is .68 and .72 respectively.

Looking back to the tuning sensitivity section the ratio of the tuning slopes, .695 and .766, are very close to the above values determined for $\frac{\Delta f_0}{\Delta f_{BP}}$, .712 and .743. By studying Figures 11-14 the effect of the delay line bandpass moving faster than the oscillator modes can be clearly seen. Also, the ratio of the two overall slopes, .784, is approximately equal to the ratio of the device delays .833.

To verify this idea further the ratio on movement of

43

the delay line bandpass versus oscillator frequencies for a given change in the bias field was determined. This was done for several points between two and four GHZ.

Figures 21-25 show the five sets of curves for the unweighed case. Figures 26-28 show the three sets for the weighed case. Table IV then summarizes the results by showing the calculated $\frac{\Delta f_0}{\Delta f_{BP}}$ ratio for each of the eight sets. The experiment is in good agreement with the hypothesis presented by Castera and expressed in Equation 22.

Consider the case when the ratio of $\frac{\Delta_0}{\Delta f_{BP}}$ is unity. This means $t_0 = 0$. Depending on the gain condition being satisfied continuous tuning would result. The delay line bandpass would move along with the oscillator modes, the ratio of tuning slopes would equal unity, and an excellent oscillator could be fabricated. Further, the delay line bandpass could be signed such that only one mode was present.

Having $t_0 = 0$ is probably not achievable but if amplifiers were selected with minimum delay and positioned to cut down on cable delays the ratio could be made closer to one. This would make the system tunable over a larger region than the one observed.

In summary there are four parameters that effect the behavior of the oscillator: one, the amount of gain available; two, the bandpass of the delay line; three, the
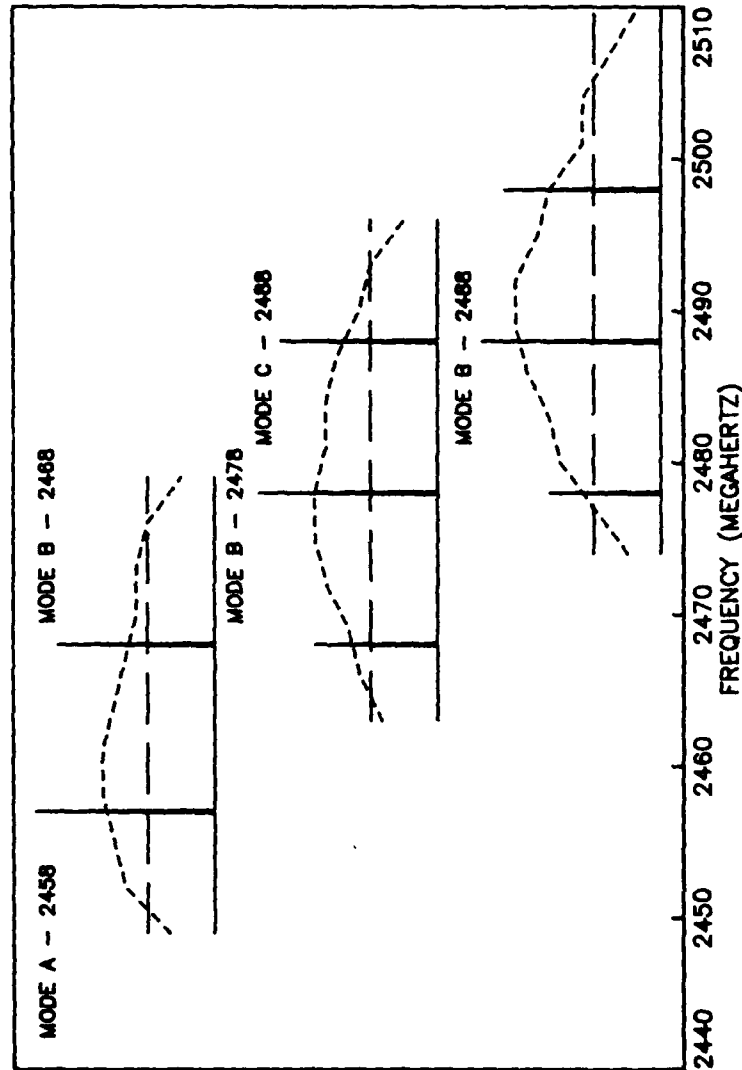
44

Figure 21. Delay Line Bandpass Versus Oscillator Spectra for Three Bias Field Strengths (Centered at 2478MHZ)

45

Figure 22. Delay Line Bandpass Versus Oscillator Spectra for Three Bias Field Strengths (Centered at 2785 MHZ).

46

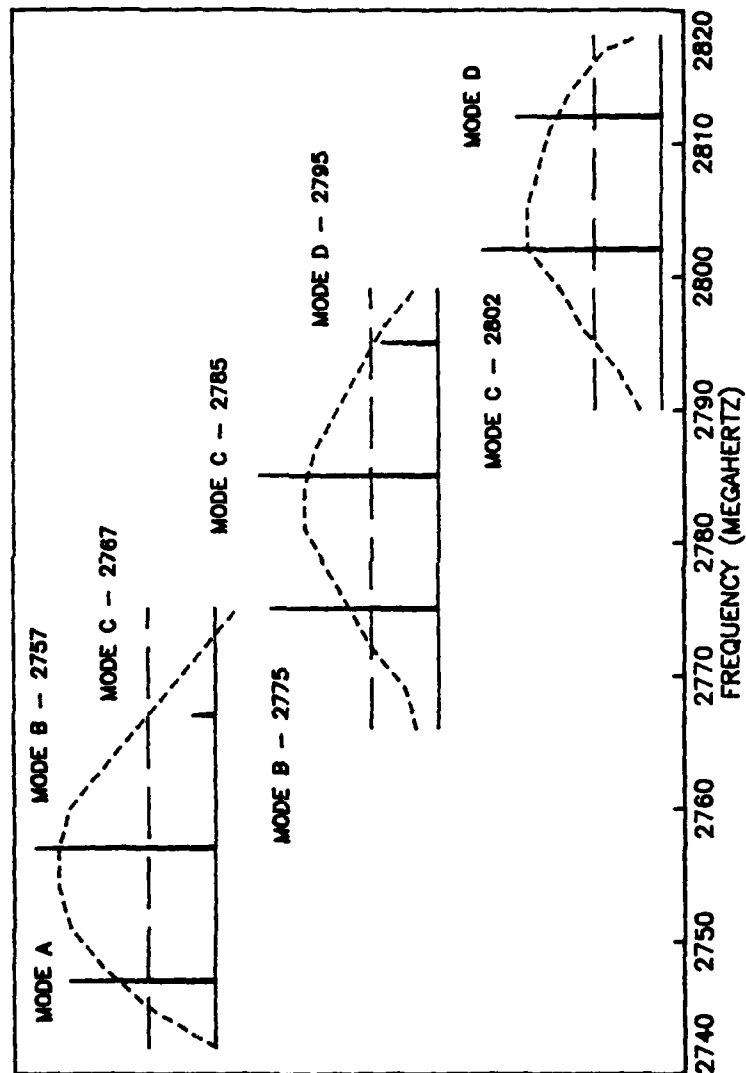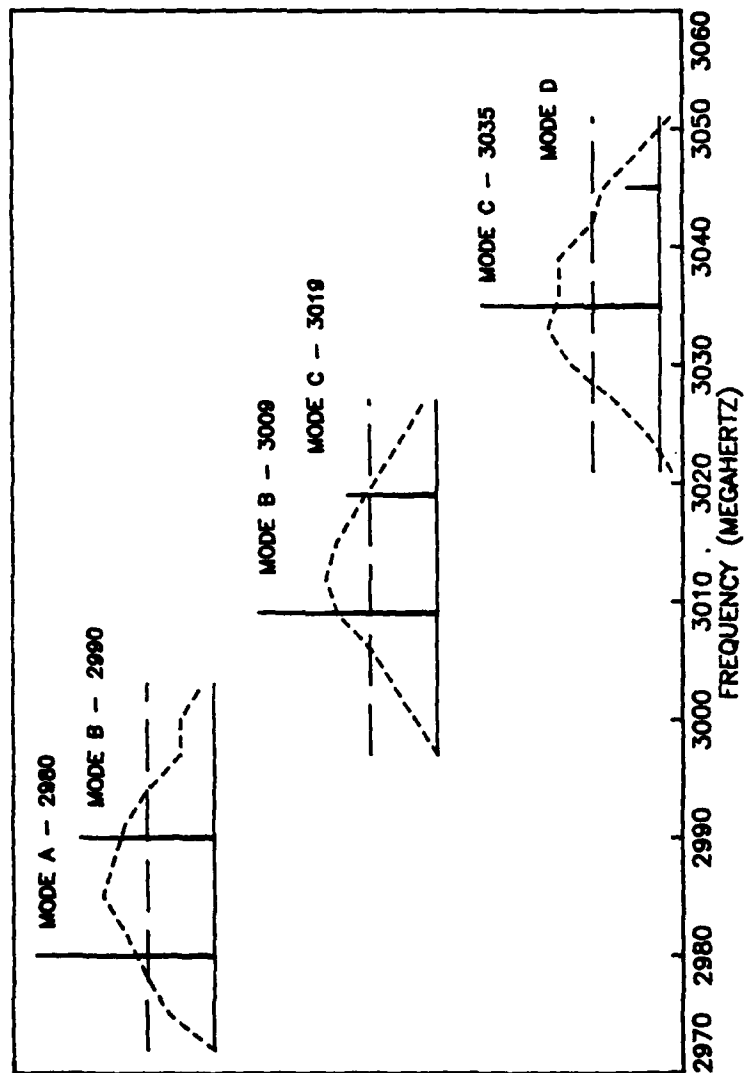Figure 23. Delay Line Bandpass Versus Oscillator Spectra for Three Bias Field Strengths (Centered at 3009 MHZ).
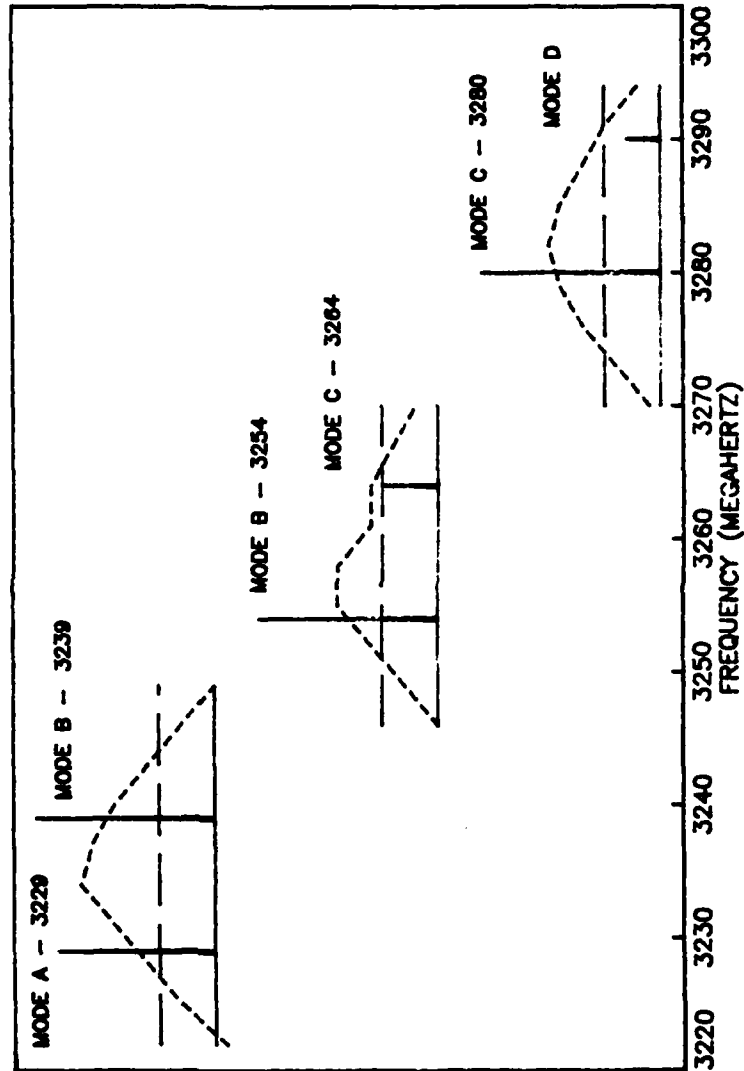
Figure 24. Delay Line Bandpass Versus Oscillator Spectra for Three Bias Field Strengths (Centered at 3254 MHZ).

48
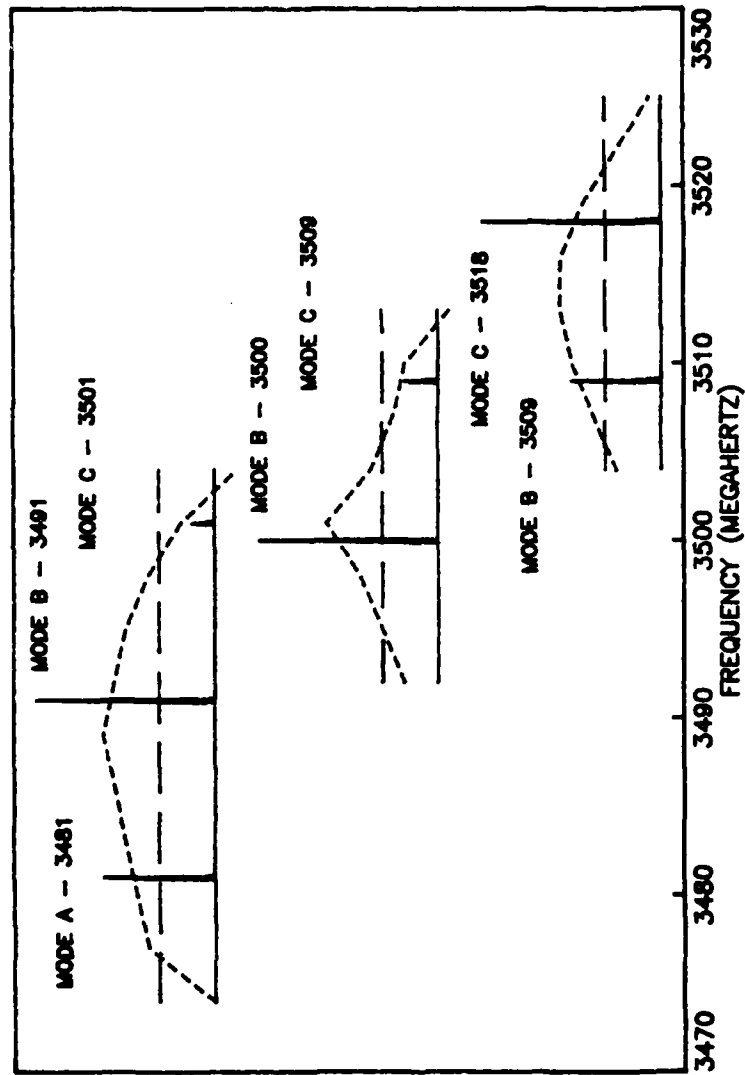
Figure 25. Delay Line Bandpass Versus Oscillator Spectra for Three Bias Field Strengths (Centered at 3500 MHZ).

Figure 26. Weighted Delay Line Bandpass Versus Oscillator Spectra for Three Bias Field Strengths (Centered at 2518 MHZ).
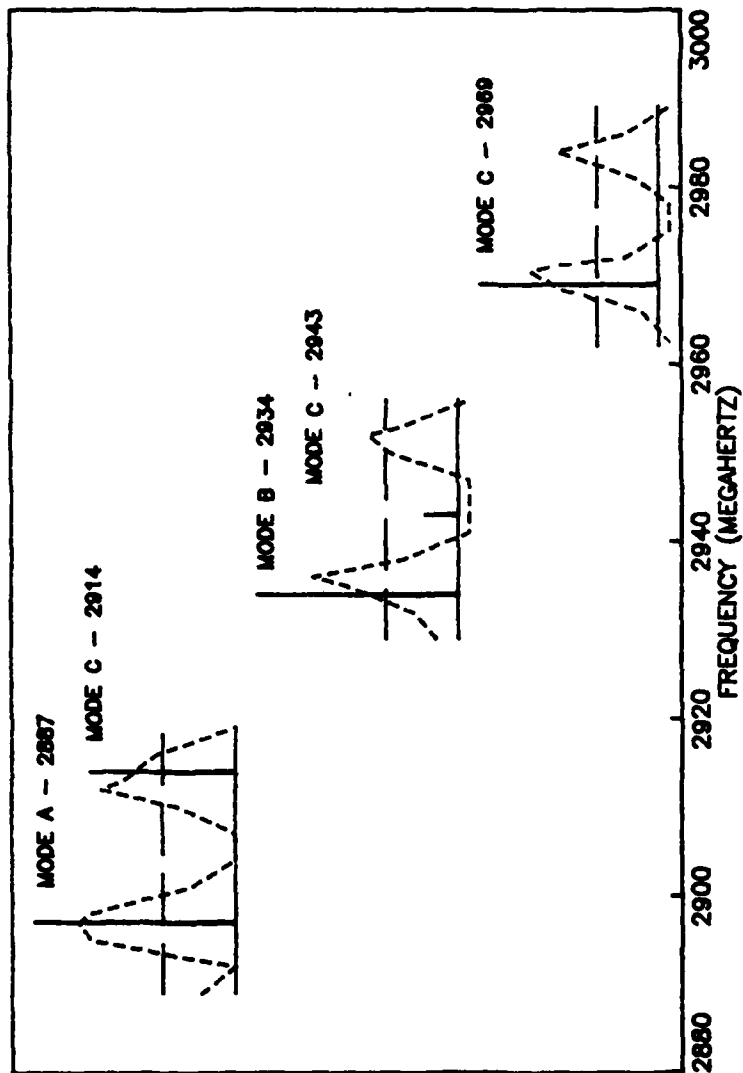
Figure 27. Weighted Delay Line Bandpass Versus Oscillator Spectra for Three Bias Field Strengths (Centered at 2934 MHZ).
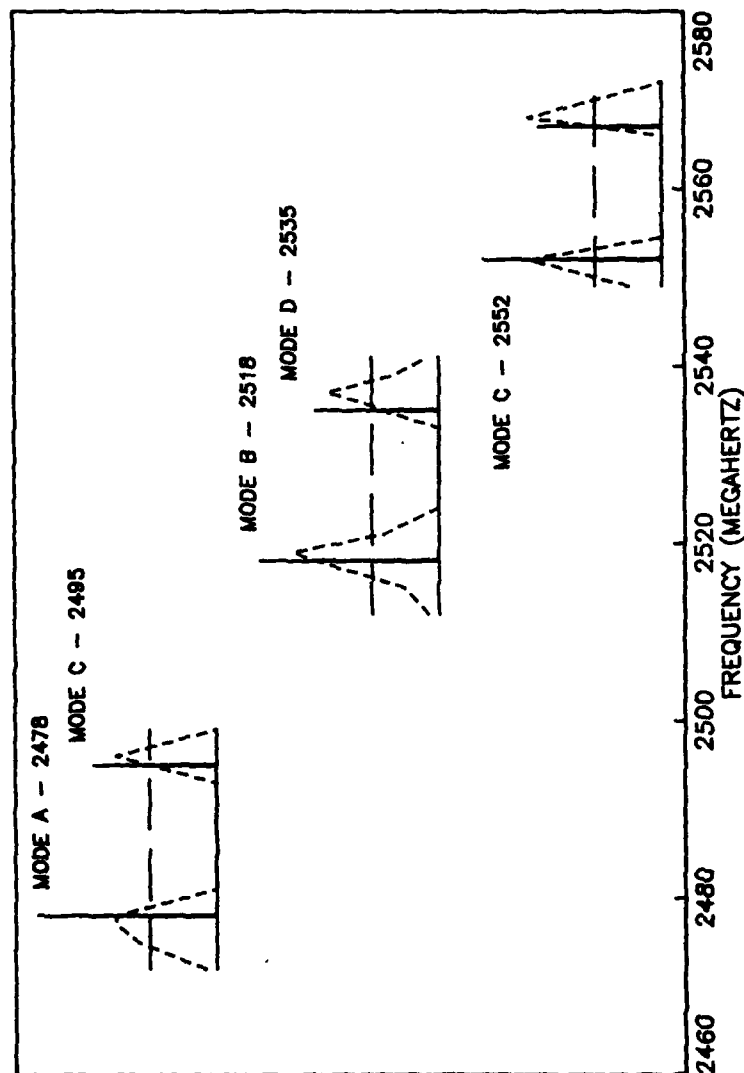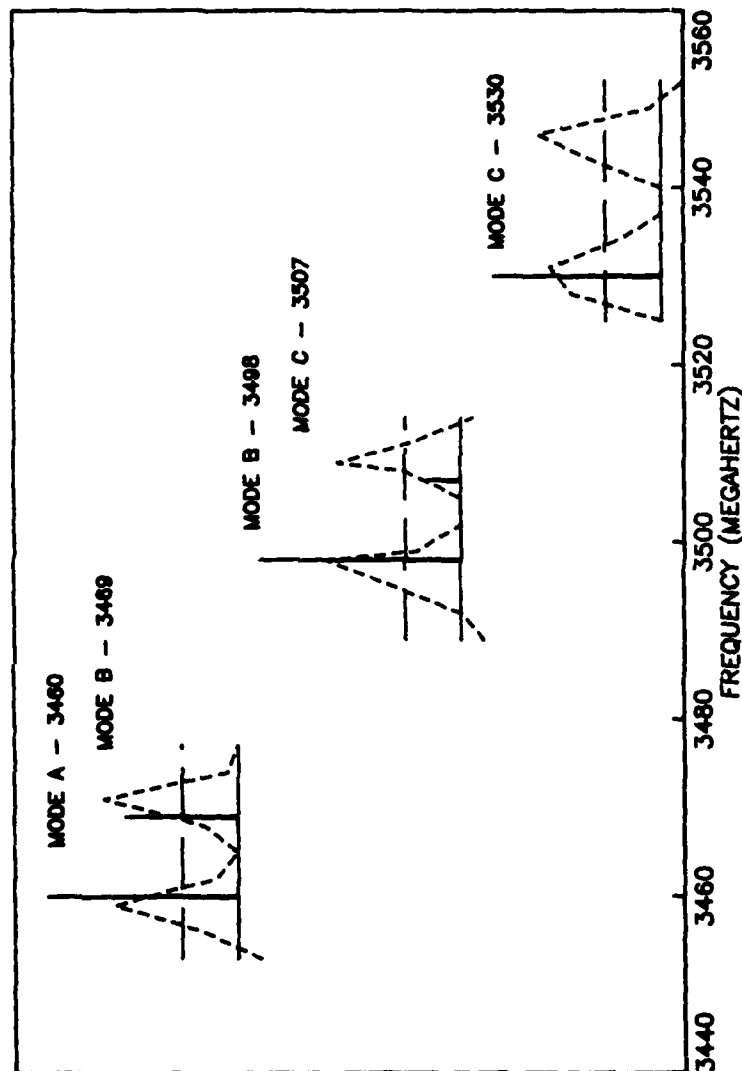
Figure 28. Weighted Delay Line Bandpass Versus Oscillator Spectra for Three Bias Field Strengths (Centered at 3498 MHZ).

TABLE IV

Change in Delay Line Bandpass verses Oscillator Frequency
(Summary of Figures 21 thru 28)

Figure	Change in Oscillator Frequency (MHz)	Change in Bandpass Frequency (MHz)	Ratio of Change in Oscillator to Bandpass	Oscillator Frequency Spacing (MHz)	Total Delay (nanosec)
21	20	29.5	.68	10	100
22	35	47	.75	10	100
23	35	48	.73	10	100
24	31	48	.65	10	100
25	19	25.5	.75	9.3	107.5
Average values for unweighted case.			.712	9.86	101.5
26	57	74	.77	9	111
27	55	73	.75	8.5	118
28	52	72	.71	9	111
Average values for weighted case.			.743	8.80	113.6

NOTE:
Device Delay calculated from average Total Delay	UW=69.2	W=81.3
Device Delay calculated from average Ratio	72.3	84.4
Device Delay calculated from ratio of slopes	70.5	87.0

53

bandwidth of the transducers; four, the amount of delay in the feedback loop. The first three parameters could not be adjusted but the delay could be increased by adding cable to the feedback loop.

Figure 29 shows the effect of adding three different length cables to the feedback loop. Remembering that $\Delta f_M = \frac{1}{\tau + t_0}$, we can expect Δf_M to decrease as delay is added. The interaction of the bandpass for the weighted delay line with the new Δf_M's and the new levels of available gain should cause the frequencies present to change. The frequency spectrum does change appreciably as delay is added. The number of modes and their spacing can clearly be adjusted by the loop delay. Table V summarizes the data presented in Figure 29.

Castera suggested that the mode hopping effect could be lessened by using two different delay paths (as shown in Figure 30). By appropriate choice of the two path lengths and the bandwidth of the transducer a single mode oscillator with a larger continuous turning range can be constructed.
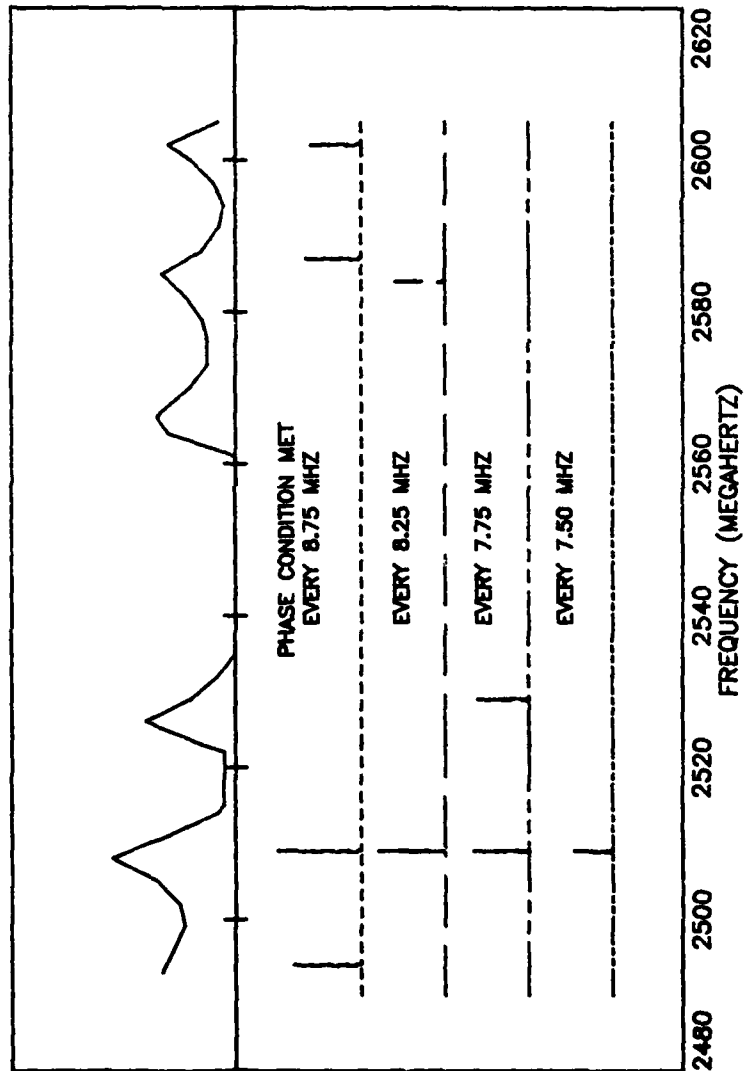
Figure 29. Effect of Additional Delay on the Weighted Delay Line Oscillator.

55

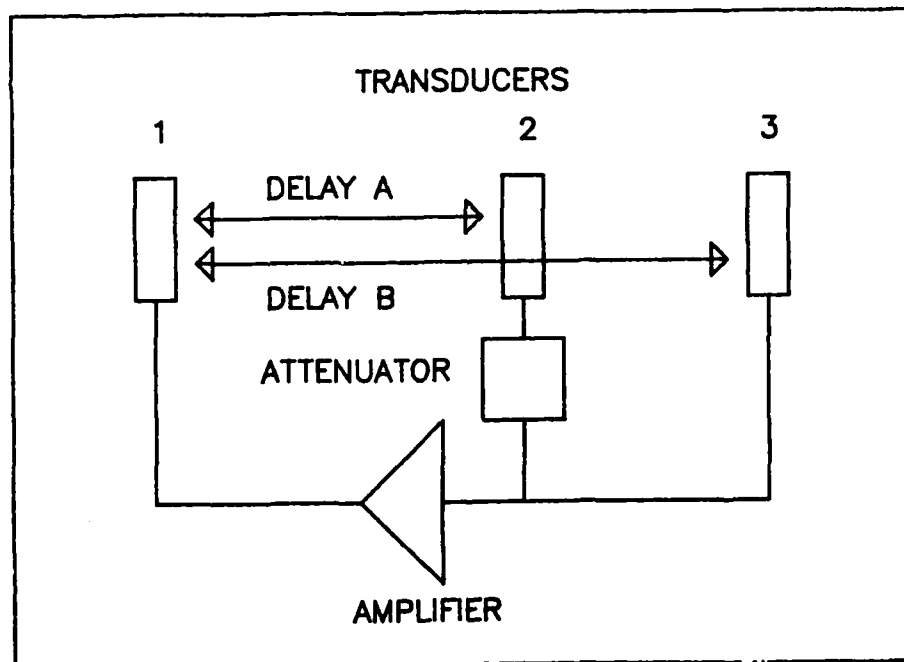| TABLE V		
Effect of Additional Delay on Oscillator Mode Spacing		
Cable Length (feet)	Mode Spacing (MHz)	Delay Added (nanosecs)
0	8.80	0.0
5	8.25	6.9
16	7.75	14.7
20	7.50	19.0

Figure 30.   Castera Multiple Path Delay Line Oscillator
Approach.

IV. Conclusion

Summary

The oscillator behavior was in good agreement with the previous work done by AFCRL and others mentioned in the introduction. The oscillator was continuously tunable over a limited frequency band before hopping to a higher mode. The size of this tuning band was determined to be a function of the bandpass of the delay line, the amount of available gain, and the type of transducers used. The total delay in the loop determines the spacing between modes. The interaction of the above four parameters as the bias field is changed causes the multimoding and mode hopping behavior.

The oscillator had a constant three dB noise bandwidth of 1.6 MHZ and the quality factor varied linearly with frequency from 1200 to 2400. This behavior was explained by the dominance of the transducer effects on the overall Q instead of material effects as in quartz crystal or surface acoustic wave devices.

The tuning sensitivity was found to be a function of the delays in the loop. Two slopes characterized the change in frequency versus bias field strength. First, an overall slope relates to the delay line bandpass's shift in frequency which is determined by the amount of delay in the delay line. The second slope refers to a segmented line which is determined by the total delay in the feedback loop.

57

For the unweighted transducer case the slopes were 3.40 and 2.42 MHZ/gauss respectively.

The best switching speed was .18 MHZ/μsec. This was 50 times slower than the switching speed for an experimentally determined band stop filter by Sethares and Tsai. In these experiments, coils were used to pulse the field, whereas Sethares and Tsai used a current strip fabricated in the device. They also used YIG disks as opposed to a rectangular YIG film. Their experiment allowed a shorter rise time and higher current handling capabilities.

The tuning rate was found to be 3120 MHZ/sec or 3.1 KHZ/μsec. Although slower than the best switching speed measured this still seems a reasonable result. Continuous versus discontinuous frequency shifting would account for slower times.

Recommendations

In order to determine the limit to the switching speed a better means must be found to change the bias field. Selfwound coils are too slow in their response. Additional work should be done to see if the bias magnetic field must exist for a finite time for oscillation to occur. This would, if true, effect the assumption of "given a current you have a corresponding frequency."

The exploration of additional transducer design should be conducted to see if a better shaped bandpass could be

58

developed. Using various delays the tuning regions could be adjusted to fit specific applications.

Components should be selected to reduce delay. Specifically, t_0 could be reduced if only one solid state amplifier was used instead of two (one of which was a traveling wave tube as in this study). Components should also be positioned as close as possible. A sufficiently redesigned experiment could confirm that if t_0 is minimized, the region of continuous tuning will increase.

Finally, this thesis concerned itself with just the surface waves. Experiments should be repeated to see if the performance measured is the same for the volume waves.

Bibliography

1. Brundle, L.K., and Freedman, N.J., "Magnetostatic Surface Waves on a Y.I.G. Slab," <u>Electronics Letters</u>, 4:132-134, 1968.

2. Carter, R.L., et al "Tunable Magnetostatic Surface Wave Oscillator at 4 GHZ," <u>Proceedings of the IEEE International Microwave Symposium</u>, 383-385, 1981.

3. Castera, J.P., "Tunable Magnetostatic Surface Wave Oscillators," <u>IEEE Transactions on Magnetics</u>, 14-5: 826-828, 1978.

4. -------- and Hartemann, P., "Magnetostatic Surface Wave Oscillators and Resonators," <u>Proceedings of the 8th European Microwave Conference</u>, 658-662, 1978

5. Damon, R.W., and Eshbach, J.R., "Magnetostatic Modes on a Ferromagnetic Slab," <u>Journal of Phys. Chemical Solids</u>, 19:308-320, 1961.

6. Ganguly, A.K., and Webb, D.C., "Microstrip Excitation of Magnetostatic Surface Waves: Theory and Experiment," <u>IEEE Transactions on Microwave Theory and Techniques</u>, 23-12:988-1006, 1975.

7. Haworth, J., "A Magnetostatic Delay Line Oscillator," <u>Proceedings of the IEEE Ultrasonics Symposium</u>, 344-347, 1973.

8. Miller, N.D.J., and Brown, D., "Tunable Magnetostatic Surface Wave Oscillator," <u>Electronics Letters</u>, 12:209-210, 1976.

9. Owens, J.M., et al. "Magnetostatic Waves, Microwave SAW?," <u>Proceedings of the IEEE Ultrasonics Symposium</u>, 506-513, 1980.

10. Paris, D.T., and Hurd, K.F., <u>Basic Electromagnetic Theory</u>, McGraw-Hill Book Company, New York, 1969.

11. Ramo, S., Whinnery, J.R., and Van Duzev, T., <u>Fields and Waves in Modern Radio</u>, John Wiley and Sons, Inc., New York, 1965.

12. Sethares, J.C., Tsai, T., and Koltunov, I., "Periodic Magnetostatic Surface Wave Transducers," Technical Report RADC-TR-78-78, 1978.

13. --------, and Stiglitz, M.R., "Magnetostatic Wave Oscillator Frequencies," _Journal of Applied Physics_, 52-3:2273-2275.

14. Soohoo, R.F., _Theory and Application of Ferrites_, Prentice-Hall, Inc., New Jersey, 1960.

15. Sparks, M., _Ferromagnetic Relaxation Theory_, McGraw Hill Book Company, New York, 1964.

16. Tsai, T. and Sethares, J.C., "Band Stop Filter Using LPE-YIG Films," _Proceedings of the IEEE Microwave Symposium_, 526-528, 1977.

17. Von Aylock, W.H., _Handbook of Microwave Ferrite Materials_, Academic Press, Inc., New York, 1965.

Appendix: Equipment

The following is a list of the equipment used during this thesis. Included is a brief description of the equipment and identification of the manufactuer.

EQUIPMENT	DESCRIPTION
Spectrum Analyzer	Alteck Model 707 tunable from 0.001 to 12 GHZ.
Oscilloscope	Textronix model 564 dual input oscilloscope. Fastest time base at .5μsecs.
Microwave Amplifier A	Hewlett-Packard HP491C (Traveling wave tube). 30dB rated output over two to four GHZ.
Microwave Amplifier B	Avantek model ABG - 4005M 35dB rated output over two to four GHZ. (damage to one stage decreased gain to 15 dB.)
Directional Coupler	Sage Laboratories model 783-10. Provided -10 dB coupling over two to four GHZ.
Variable Attenuator	Navda model 792FM. Provided continuously adjustable uncalibrated attenuation over two - four GHZ.
Phase Shifter	Navda model 3752. Provided phase variation over one to five GHZ.

62

|	
Sweep Oscillator	Hewlett Packard HP 692D. Provided manual or automatic tuning over two - four GHZ.
Delay Line	Two magnetostatic delay lines provided by AFCRL.
Gauss Meter	Bell Model 240. Provided measure of DC and incremental magnetic fields from 0.1 to 30,000 Gauss.
Waveform Generator	Wavetek model 111. Provided sine and square wave from 0.01 to 100,000 Hertz.
Power Amplifier	Hewlett Packard HP467A. Provided variable gain of 0-20 dB over five to 1,000,000 Hz.
Laboratory Electromagnet	Atomic Laboratories DC electromagnet. (Provided DC power supply).
Power Supply	Electronic Measurements SCR model 10. Provided 0-five Amps over 0-300 volts DC. (Used to power electromagnet).
Delay Line Mount	Three axis translator used to position delay line in biasing field. (Manufactured locally).
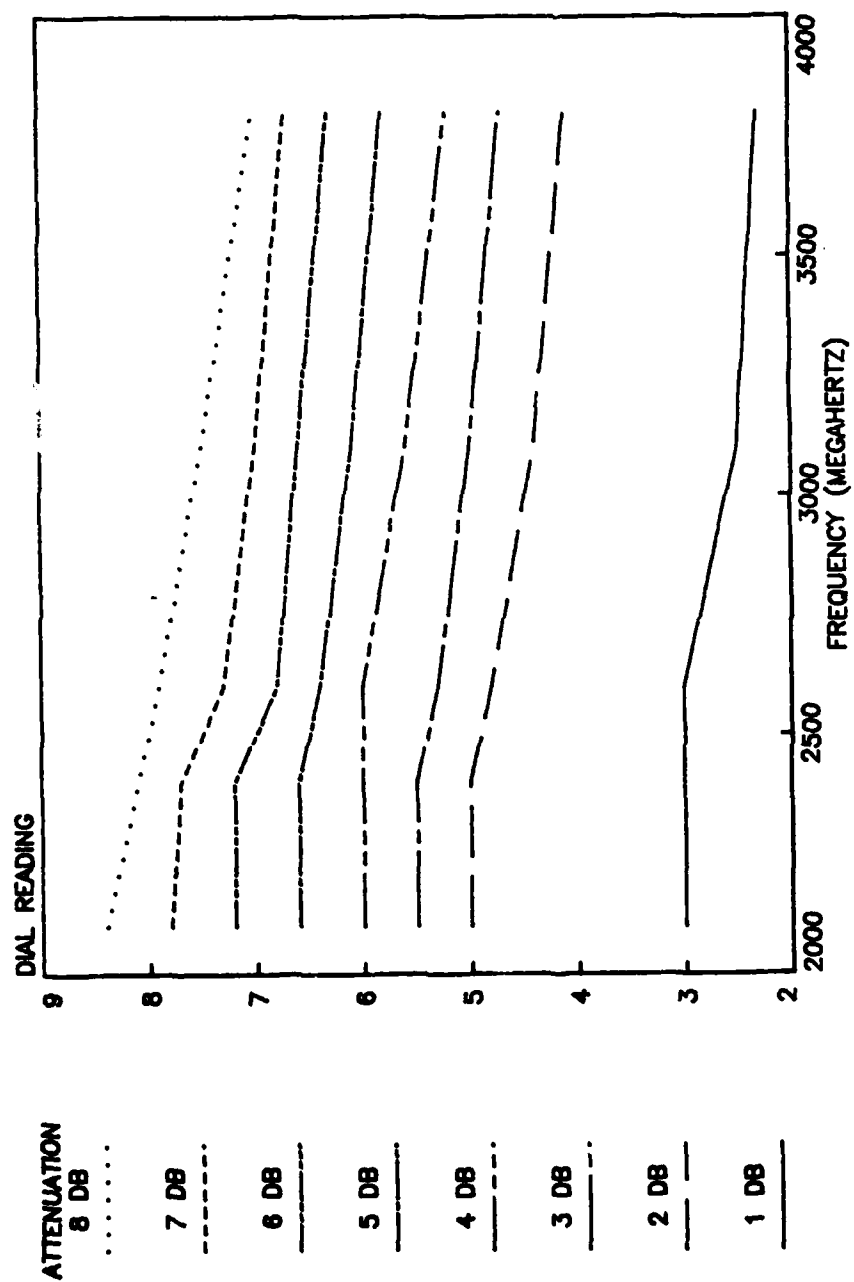
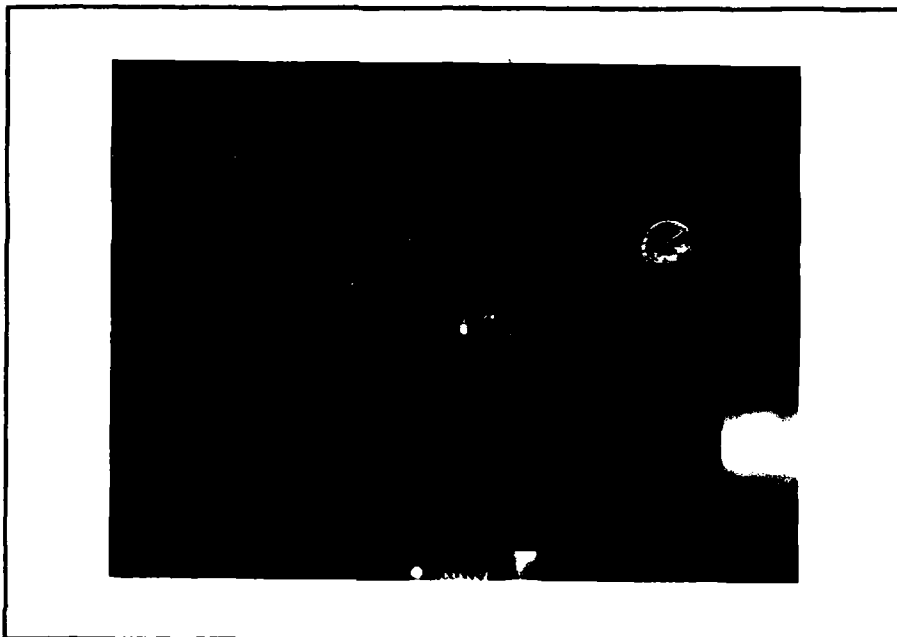Figure 31. Calibration Curve for Variable Attenuator.

64

Figure 32. Top View of DC Electromagnet
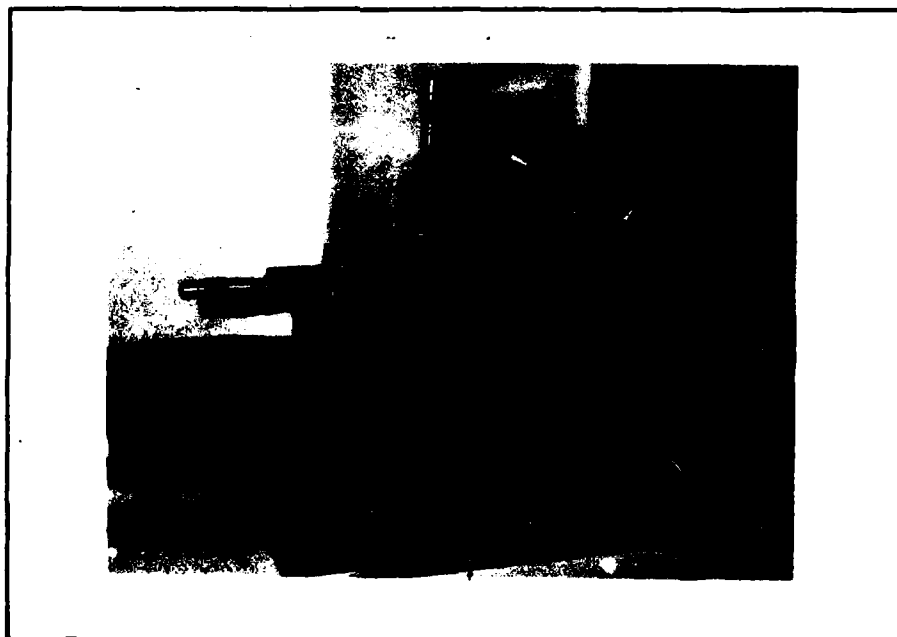and Device Positioning Assembly.

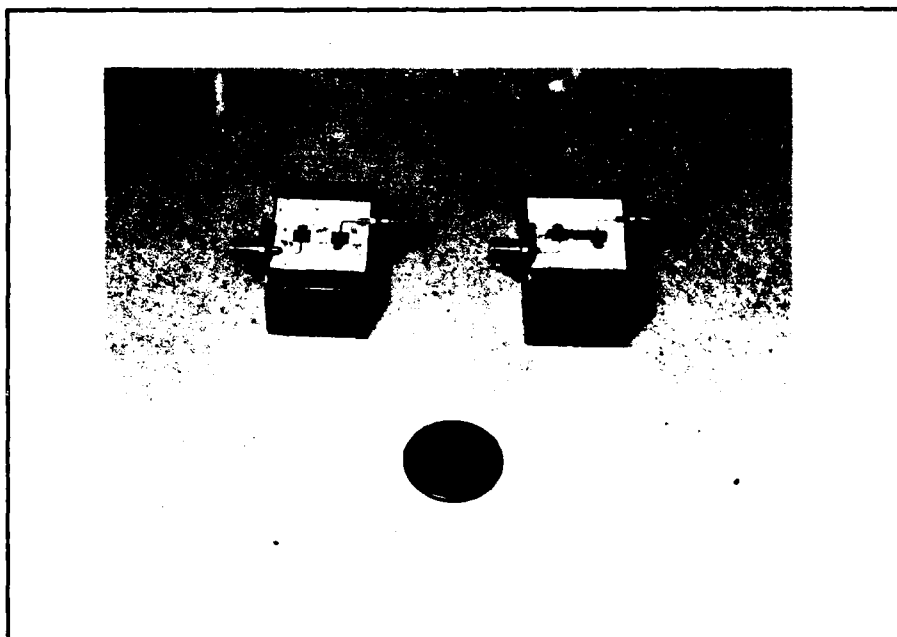Figure 33. Front View of DC Electromagnet
and Device Positioning Assembly.

Figure 34.   Unweighted and Weighted Delay Lines.

VITA

Philip W. Linke was born on 28 October 1951 in Point Pleasant, New Jersey. He attended Stevens Institute of Technology in Hoboken, N.J., and was commissioned in May 1974 through the Air Force Reserve Officer Training Program. Following commissioning he completed Undergraduate Navigator Training and Electronic Warfare Training in December 1975 at Mather Air Force Base, California. He was then assigned to the 7th Bomb Wing, Strategic Air Command, Carswell AFB, Texas where he served as a B52D crew member and instructor. In June, 1980 he entered the Air Force Institute of Technology where his studies will lead to a master of science degree in electrical engineering specializing in electronic warfare systems.

Permanent Address: 3 Evergreen Avenue
Sea Girt, N.J. 08750

SECURITY CLASSIFICATION OF THIS PAGE *(When Data Entered)*

REPORT DOCUMENTATION PAGE		READ INSTRUCTIONS BEFORE COMPLETING FORM
1. REPORT NUMBER AFIT/GE/EE/81D-35	2. GOVT ACCESSION NO. AD-A115 583	3. RECIPIENT'S CATALOG NUMBER
4. TITLE *(and Subtitle)* Magnetostatic Surface Wave Microwave Oscillator		5. TYPE OF REPORT & PERIOD COVERED MS Thesis
		6. PERFORMING ORG. REPORT NUMBER
7. AUTHOR(s) Philip W. Linke, Captain, USAF		8. CONTRACT OR GRANT NUMBER(s)
9. PERFORMING ORGANIZATION NAME AND ADDRESS Air Force Institute of Technology (AFIT-EN) Wright-Patterson AFB, Ohio 45433		10. PROGRAM ELEMENT, PROJECT, TASK AREA & WORK UNIT NUMBERS
11. CONTROLLING OFFICE NAME AND ADDRESS Antennas and R. F. Components Branch Electromagnetic Sciences Division Rome Air Development Center, Hanscom AFB, MA 01731		12. REPORT DATE December 1981
		13. NUMBER OF PAGES 80
14. MONITORING AGENCY NAME & ADDRESS*(if different from Controlling Office)*		15. SECURITY CLASS. *(of this report)* Unclassified
		15a. DECLASSIFICATION/DOWNGRADING SCHEDULE

16. DISTRIBUTION STATEMENT *(of this Report)*

Approved for public release; distribution unlimited.

17. DISTRIBUTION STATEMENT *(of the abstract entered in Block 20, if different from Report)*

18. SUPPLEMENTARY NOTES

Approved for public release IAW AFR 190-17

FREDERIC C. LYNCH, Major, USAF
Director of Public Affairs

15 APR 1982
Dean for Research and Professional Development
Air Force Institute of Technology (ATC)
Wright-Patterson AFB, OH 45433

19. KEY WORDS *(Continue on reverse side if necessary and identify by block number)*

Microwave oscillators
Magnetostatics and propagation

20. ABSTRACT *(Continue on reverse side if necessary and identify by block number)*

This thesis presents an experimental analysis of a magnetostatic surface wave delay line used in a two-four gigahertz feedback loop oscillator. The analysis focused on the multimoding and mode hopping effects. The tuning rate, switching speed and quality factor were also examined.

The results showed that the mode hopping behavior is a result of the interaction of the delay line delay and the total loop delay. The multimoding behavior was found to be a function of the loop gain and the delay line's

DD FORM 1473 EDITION OF 1 NOV 65 IS OBSOLETE

SECURITY CLASSIFICATION OF THIS PAGE *(When Data Entered)*

insertion loss, bandpass and delay. Two approaches to help reduce these undesirable effects were outlined.

ATE
LME